Uplift of the Altiplano-Puna plateau: A view from the west

T. E. Jordan,[1] P. L. Nester,[1] N. Blanco,[2] G. D. Hoke,[3] F. Dávila,[4] and A. J. Tomlinson[2]

Received 5 January 2010; revised 24 May 2010; accepted 7 June 2010; published 15 September 2010.

[1] The western flank of the Central Andean Plateau is a crustal-scale monoclinal fold, expressed in the geomorphology and in the westward tilt of fore-arc basin strata. Data from three fore-arc basins quantify the magnitude and time of displacement of the plateau system relative to the fore arc. From 18°30′S to 22°S there is a single monocline strand. There, other authors documented ~2000 m (±500 m) of early and middle Miocene structural relief growth across small-scale monoclines, and our data reveal 810 m (±640 m) of ~11–5 Ma relief growth and 400 m (±170 m) relief growth since ~5 Ma across a long-wavelength monoclinal fold limb. This structural relief growth since ~11 Ma approximates the topographic relief growth between the fore arc and the Altiplano plateau. From 22°S to 24°S there are two subparallel long-wavelength monoclines. Structural relief on the east side of the fore arc increased by 2840 m (±2510 m) during ~17–10 Ma and by 2320 m (±1050 m) since ~10 Ma. Some part of this monoclinal limb rotation led to topographic uplift of the adjacent Puna plateau. Rotation across the western monocline could have increased the altitude of the fore-arc basins by <900 m since ~6 Ma and may result from intense heating of the eastern margin of the cold and strong Atacama lithosphere block. Although the wavelengths of the monoclines vary along strike and through time, the monoclinal style of deformation dominated the uplift history of the eastern fore arc of the central Andes throughout the Neogene. **Citation:** Jordan, T. E., P. L. Nester, N. Blanco, G. D. Hoke, F. Dávila, and A. J. Tomlinson (2010), Uplift of the Altiplano-Puna plateau: A view from the west, *Tectonics*, *29*, TC5007, doi:10.1029/2010TC002661.

1. Introduction

[2] The central Andes are the largest positive topographic feature of Earth's continents that is not associated with plate collision [*Isacks*, 1988]. The primary highstanding sector is the Central Andean Plateau, a region (350–400 km wide by 1800 km long) that is above ~3000 m elevation, which encompasses the Western Cordillera, Altiplano-Puna plateau, and Eastern Cordillera physiographic provinces (Figure 1) [*Allmendinger et al.*, 1997]. We probe the uplift history of the Altiplano-Puna plateau surface by examining the Neogene history of relief development across the western flank of the Andes.

[3] The Altiplano-Puna province is a region characterized by closed drainage between two marginal uplands. The Western Cordillera, defined by the positions of stratovolcanoes of Miocene and younger age at the western margin of the Altiplano-Puna province, has peaks that rise to ~6000 m elevation. The Eastern Cordillera, a 5000–6000 m elevation range east of the Altiplano-Puna highland surface, is deeply exhumed and hosts extensive Cenozoic fault systems [*Horton*, 2005; *Gillis and Horton*, 2006; *Hongn et al.*, 2007]. The broad, low-relief Altiplano, north of 22°S, has a mean elevation of ~3800 m, whereas the basin-and-range morphology Puna, south of 22°S, has a mean elevation of ~ 4400 m (Figure 1) [*Whitman et al.*, 1996]. The constructional volcanic peaks contribute greatly to relief within the Western Cordillera (Figure 2), but those peaks are perched on top of the same low-relief landform that stretches across the Altiplano-Puna domain [*Isacks*, 1988].

[4] An important part of explaining the physical controls on uplift of the central Andes is to document the timing and magnitude of formation of regional topographic relief between the plateau and the fore arc (Figures 2, 3, and 4). Because the units that serve as kinematic marker horizons in the fore arc and on the western margin of the Altiplano-Puna are ~25 Ma and younger, we limit our analysis to relief development during the Neogene. This paper analyzes the history of relief development based on new data and previous studies, and relates this history to major tectonic phenomena.

[5] Between ~18°S and 24°S latitude, today's topographic highlands of the western plateau and fore arc are a product of a suite of phenomena: (1) pre-Neogene topographic relief, remnant from Paleogene and older tectonic activities which erosion has not entirely erased; (2) construction of volcanic edifices over the Earth's surface; (3) short-wavelength (~1 km limb width) monoclinal structural relief formation across upper crustal faults and folds; (4) long-wavelength monoclinal (~30–50 km limb width) relief formation; (5) very long-wavelength (>50 km) relief development and tilt of the Atacama lithospheric block; and (6) rock uplift of the entire fore arc and mechanically connected Andes. We consider the latter four phenomena to be direct expressions of Neogene tectonic activity. We first document the style, magnitude and timing of Neogene relief development, and then discuss the phenomena that underlie

[1]Earth and Atmospheric Sciences, Cornell University, Ithaca, New York, USA.
[2]Servicio Nacional de Geología y Minería, Santiago, Chile.
[3]Earth Sciences, Syracuse University, Syracuse, New York, USA.
[4]Cátedra de Estratigrafía y Geología Histórica, Universidad Nacional de Córdoba, Córdoba, Argentina.

0278-7407/10/2010TC002661

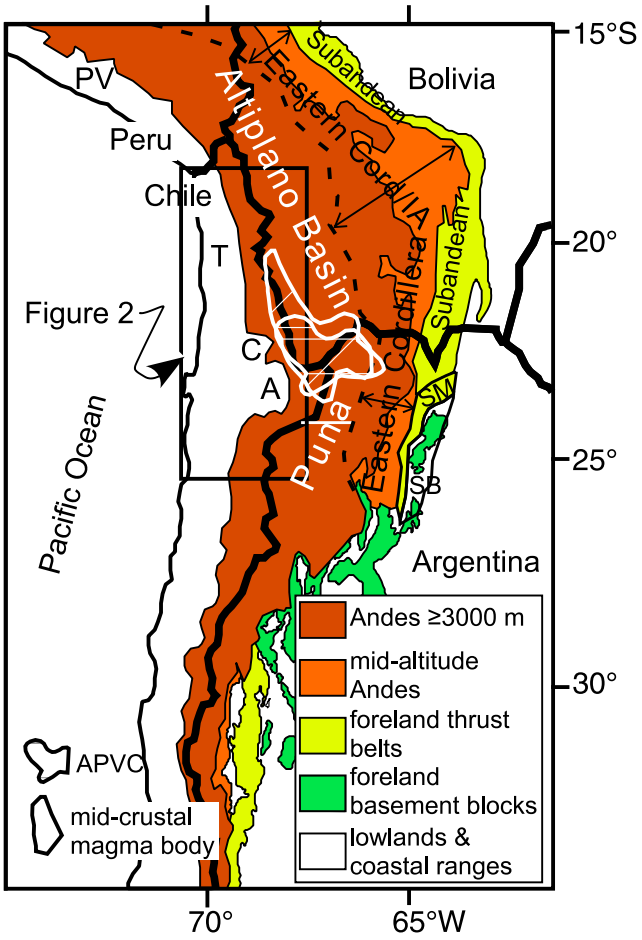

Figure 1. Location map of the Central Andes Mountains in western South America. The Central Andean Plateau is indicated by the wide region above 3000 m elevation that is north of ~27°S. The border between Argentina and Bolivia approximates the boundary between the Altiplano and Puna segments of the plateau. A thin white line approximates the boundary between the northern and southern Puna. Chile's eastern national boundary approximates the position of the volcanic arc and Western Cordillera. Colors distinguish the foreland provinces. The undifferentiated Eastern Cordillera and Interandean Zone (I/A) span the eastern part of the plateau and Andean slopes descending to the east. The most extensive young thrust belt is the classic thin-skinned Subandean thrust belt. To its south two zones with distinctive deformation styles, the Meridional Subandean belt (SM) and the Santa Barbara System (SB), grade to the crystalline basement uplifts of the Sierras Pampeanas south of 27°S latitude. T, C, and A mark the positions of the Tamarugal, Calama, and Atacama basins, respectively. Compiled from *Allmendinger et al.* [1997], *Horton* [2005], and *Rosario et al.* [2008]. The positions of the Altiplano-Puna Volcanic Complex (APVC), defined by 10–1 Ma ignimbrites and calderas [*de Silva*, 1989], and of a seismologically defined zone of partial melt at 17–19 km depth in the crust [*Zandt et al.*, 2003] are marked.

the fourth and fifth categories, the long-wavelength and very long wavelength fore-arc tilting.

[6] Whereas volcanoes and short-wavelength deformation are widely recognized to control the major geomorphological features of fore-arc and arc regions, monoclines exceeding tens of kilometers in width and of kilometer-scale relief are not associated in the literature with fore arcs [*Isacks*, 1988]. We demonstrate that the monoclinal kinematic style on the western flank of the central Andes is not only spatially persistent [*Isacks*, 1988] despite local variability, but also temporally long-lived. We speculate that this style, although rarely preserved, may be a common upper crustal style at the boundary between arc and fore arc.

[7] It should be noted that the western Andean slope is a highly unusual mountain front because much of it lies in the hyperarid Atacama (Chile) and Sechura (Peru) deserts. These are so arid that the rate of degradation of the landscape by surface processes is extraordinarily slow except in narrow canyons. Between the canyons, broad regions exist with very little local surface relief, termed "pediplains." On these pediplains the scale of local vertical relief generated by the combination of erosion and deposition over a period in excess of 10 Myr is less than ~10 m [*Nishiizumi et al.*, 2005; *Kober et al.*, 2006; *Evenstar et al.*, 2009]. Consequently, the landforms of the pediplains at vertical scales exceeding ~10 m reflect the accumulation of almost pure tectonic and/or volcanic activity. This lack of surface erosion provides unique opportunities to document surface uplift magnitude and upper crustal kinematic style.

2. Prior Studies of Uplift of the Central Andes

[8] Two types of studies have partially quantified surface uplift of the central Andes. A set of proxy studies of surface deposits within the Altiplano document paleotemperature (fossil leaf physiognomy and Δ-47 of carbonates [*Charrier et al.*, 1994; *Gregory-Wodzicki*, 2000, 2002; *Ghosh et al.*, 2006; *Garzione et al.*, 2006, 2008; *Quade et al.*, 2007] and/or paleo-isotopic composition of soil water [*Garzione et al.*, 2006, 2008; *Quade et al.*, 2007]. On the assumption that modern variations of temperature and of meteoric water isotopes with elevation held in the past, paleo-altitudes of the depositional surface can be deduced. These studies in general conclude that the Altiplano was a low-elevation (~1000 m) region during the Oligocene, modestly higher (1000–2000 m) during the middle Miocene, rose during the late Miocene to become a very high plateau (3500–4000 m), and has changed little in altitude during the Plio-Quaternary. The elevation estimates from these proxies are subject to errors related to the difference between paleoclimate at the time the proxy was incorporated into a rock and today's climate [*Ehlers and Poulsen*, 2009]. *Barnes and Ehlers* [2009] point out that an opposing interpretation, that the pace of uplift of the Altiplano has been steady throughout the last 25 Ma, is equally consistent with the uncertainties on the proxy data.

[9] A second set of studies has measured the relief development across the Western Andean Slope, between points in the lowland fore-arc basin west of the Andes and the western rim of the Altiplano. These studies use the

distribution and facies of strata in the fore-arc basins [e.g., *Charrier et al.*, 2007; *Hartley and Evenstar*, 2010] or use marker horizons whose original surface continuity or inclination can be estimated (e.g., surface deposits or geomorphic surfaces) [*Wörner et al.*, 2002; *Victor et al.*, 2004; *Farías et al.*, 2005; *Kober et al.*, 2006; *Hoke et al.*, 2007]. These studies, generally, are suggestive that there existed a highland in the area of the Altiplano during the Oliogocene [*Horton et al.*, 2001; *Charrier et al.*, 2007; *Hartley and Evenstar*, 2010], that ~1700 m of surface relief was generated between the western Altiplano and fore arc during the early and middle Miocene [*Farías et al.*, 2005], and that an additional ~1100 m relief was added during the late Miocene-Pliocene [*Hoke et al.*, 2007]. *Schildgen et al.* [2009b] determined a similar interval of time over which the western margin of the Central Andean Plateau of southwestern Perú underwent surface uplift, and they suggested that in Perú there may have been less than 1000 m of middle Miocene uplift and greater than 1400 m of late Miocene and Pliocene relative uplift.

[10] Two major unknowns of surface elevations in the system of Altiplano-Puna plateau and Western Andean Slope exist. First, *Hoke and Garzione* [2008] presented evidence that the age of Neogene uplift of the Western Cordillera and the central Altiplano might not be equivalent, and they suggested that much of the Western Cordillera uplift (early and middle Miocene) pre-dated the major uplift of the central Altiplano (late Miocene) [e.g., *Charrier et al.*, 2007; *Hartley and Evenstar*, 2010]. Given uncertainties of chronology and proxies, work remains before one can be fully confident of, or explain, quantitative differences between uplift of the western Andean slope (our focus) and the central part of the Altiplano. We contribute by quantifying the history of relief development between the western Altiplano plateau surface and the fore arc. Second, despite their similar altitudes and internal drainage, there are numerous major differences between the crust, lithosphere, asthenosphere, and magmatic history of the Altiplano and of the Puna [e.g., *Whitman et al.*, 1996; *Allmendinger et al.*, 1997; *Beck and Zandt*, 2002; *Trumbull et al.*, 2006], which lead to the expectation that their timing and magnitudes of uplift might differ. The Altiplano is dominated by a broad central basin at ~3800 m above sea level, little Plio-Pleistocene magmatic activity east of its western margin, a 70–80 km thick felsic crust, and a lithospheric mantle as thick as 125–150 km, as suggested by high Vp and Vs and moderately high Q in the shallow mantle [*Myers et al.*, 1998]. In contrast, the Puna has a basin-and-range landscape, mean elevation ~4400 m above sea level, widespread Plio-Pleistocene volcanic activity, a crust that varies locally from 40 to 70 km thick, and a high degree of attenuation of seismic waves (Q) below the

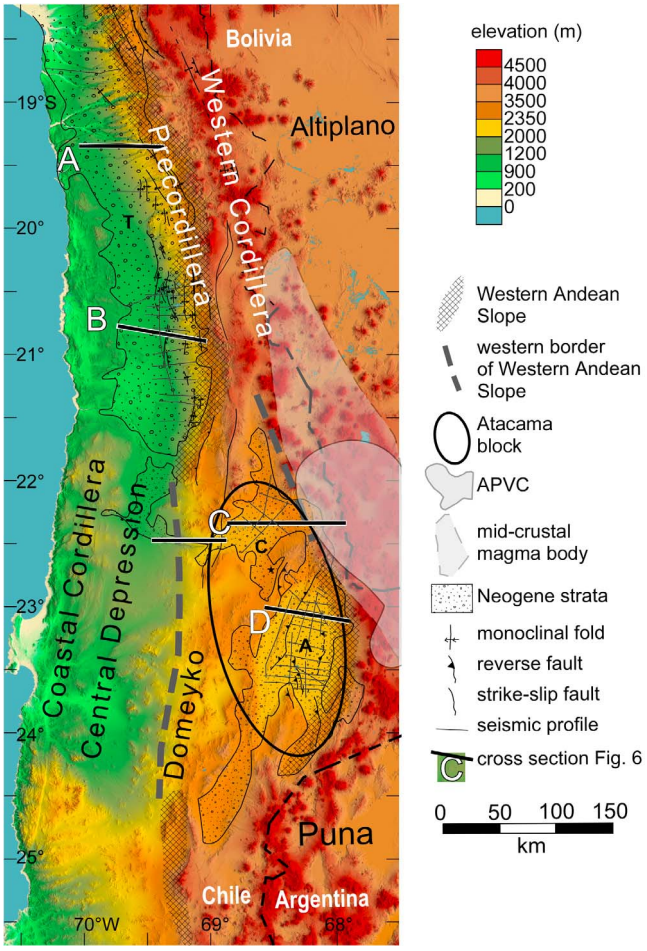

Figure 2. Shaded relief digital elevation map of the study area. Areas of long-wavelength slope to the west are indicated by cross-hatch where there is strong along-strike continuity of slopes of 3–5% inclination; a wide dashed gray line marks the western side of areas with less continuity or gentler slopes (see Figure 3 for source data). Note that elevation color boundaries are not in equal steps, but rather highlight specific parts of the landscape. Areas with more than ~50 m thickness of Neogene sedimentary rocks are mapped and mark the fore-arc basins. Profiles A and B transect the Pampa del Tamarugal basin, C transects the Calama basin, and D transects the Salar de Atacama basin (see Figure 6). The Atacama block of cold, strong lithosphere is enclosed by an oval [*Schurr and Rietbrock*, 2004]. The mapped faults and folds have experienced offset younger than ~23 Ma (based on the authors' observations and modified from *Blanco* [2008], *Blanco and Tomlinson* [2006, 2009], *Farías et al.* [2005], *García and Hérail* [2005], *Jordan et al.* [2007], *Muñoz* [2007], *Nester* [2008], *Pananont et al.* [2004], *Pinto et al.* [2004], *Ramírez and Gardeweg* [1982], *Tomlinson and Blanco* [1997], *Tomlinson et al.* [2001], and *Victor et al.* [2004]). West verging reverse faults and short-wavelength monoclinal folds capable of building laterally extensive topographic uplifts are common west of the Altiplano, but most faults west of the Puna are either strike-slip faults (no teeth) or are east vergent. The positions of the Altiplano-Puna Volcanic Complex (APVC) [*de Silva*, 1989] and of a seismologically defined zone of partial melt at 17–19 km depth in the crust (Altiplano Puna magma body) [*Zandt et al.*, 2003] are marked. Star in SE corner of the Calama basin marks the region studied by *Rech et al.* [2006].

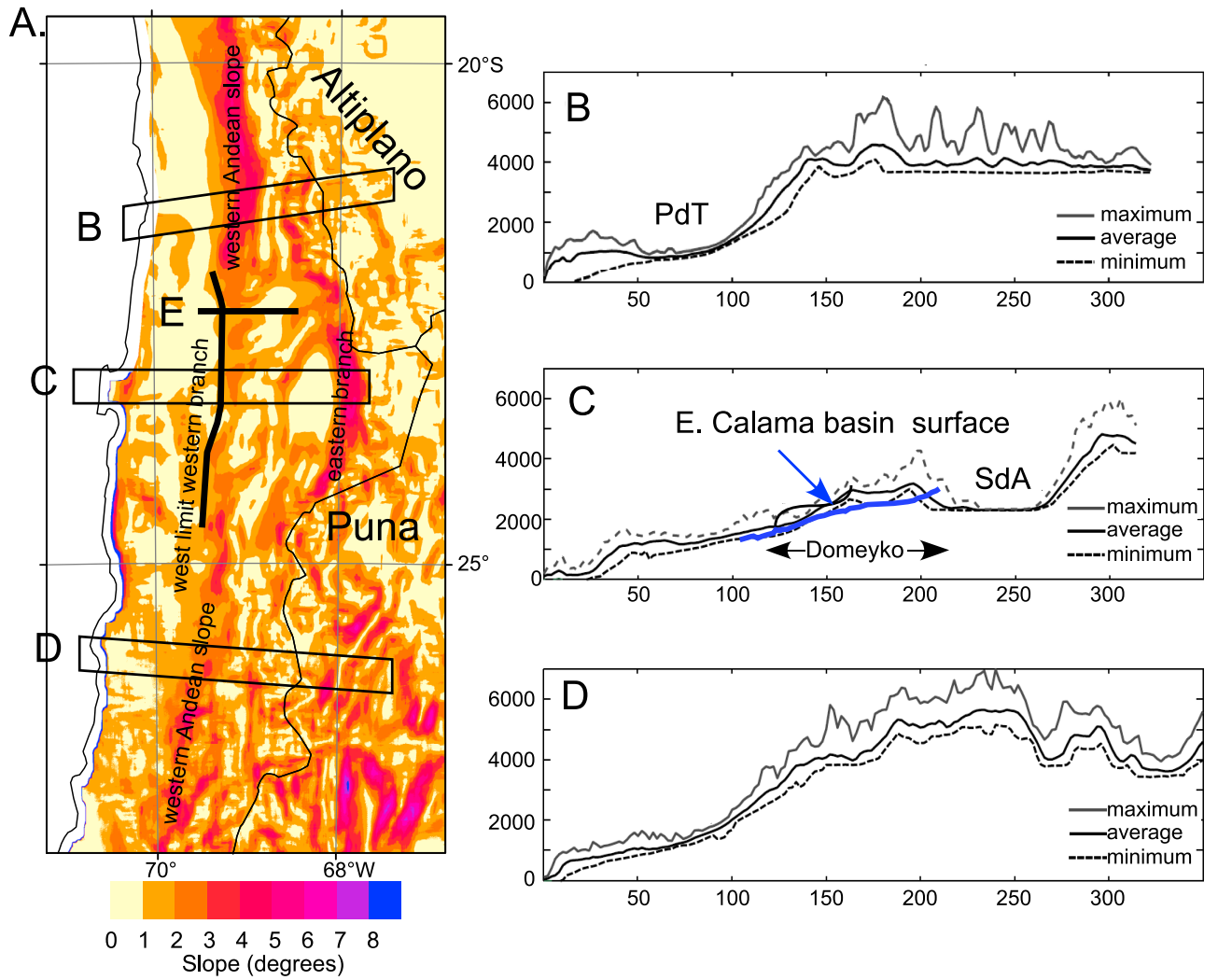

Figure 3. (a) Topographic slope map (slope of 3 × 3 pixel moving window, for pixels of 21 × 21 km whose mean elevations are derived from SRTM data) [*Hoke*, 2006]. (b, c, and d) The 40-km-wide swath topographic profiles [*Hoke*, 2006] for swaths shown in Figure 3a, corresponding to Pampa del Tamarugal (PdT) and western slope of the Altiplano (Figure 3b), profile across the Atacama-Calama block, Salar de Atacama basin (SdA), and western slope of the northern Puna (Figure 3c), and the fore arc where there is no major sedimentary basin and the western slope of the southern Puna (Figure 3d). (e) Superimposed on the swath in Figure 3c, a blue line marks a profile along the top of the Pliocene Opache Limestone through the Calama basin (line "E" on Figure 3a).

crust that suggests the mantle lithosphere is thin or absent [*Whitman et al.*, 1996; *McGlashan et al.*, 2008]. Although hypotheses based on the magmatic and deformation histories of the two parts of the plateau system invoke, in some cases, different mechanisms for their uplift [*Allmendinger et al.*, 1997; *Hindle et al.*, 2005; *DeCelles et al.*, 2009], perceptions of their uplift histories tend to converge [e.g., *Garzione et al.*, 2008; *Barnes and Ehlers*, 2009]. This paper demonstrates similarities in the timing of uplift but differences in the uplift styles of the southern Altiplano compared to the northern Puna.

[11] Most studies of the Western Andean Slope have quantified relief development across a set of short-wavelength monoclinal folds (Figure 2), whose principal time of activity was the early and middle Miocene [*Muñoz and Charrier*, 1996; *Victor et al.*, 2004; *Pinto et al.*, 2004; *García and Hérail*, 2005; *Farías et al.*, 2005; *Muñoz*, 2007]. Likewise, regional relief formation by a long-wavelength monoclinal uplift was also recognized [*Isacks*, 1988; *Wörner et al.*, 2002; *Farías et al.*, 2005; *Schildgen et al.*, 2007, 2009a, 2009b], but its age and magnitude have been most directly quantified by *Hoke et al.* [2007], who used stream profiles to estimate that ~1100 m of surface relief developed since 10 Ma. Recently, *Evenstar et al.* [2009] pointed out that a regional geomorphic surface that is key to the chronological constraints used by *Hoke et al.* [2007] is not entirely of a single age. Consequently, *Evenstar et al.* [2009] warn that the *Hoke et al.* [2007] uplift history ought to be scrutinized again. The data

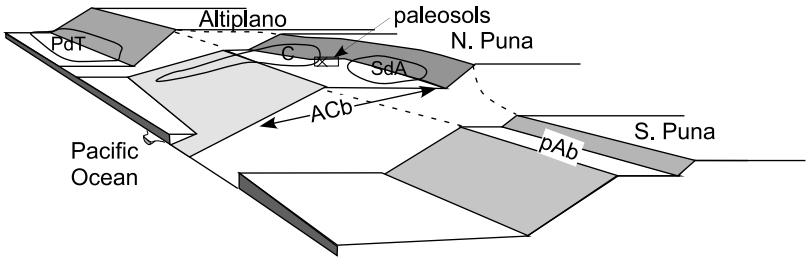

Figure 4. Perspective cartoon showing distribution of landscape zones with long wavelength slope across which the Andes Mountains reaching their topographic differentiation from the fore-arc lowlands. The positions of the sedimentary basins described in this paper are shown schematically (PdT, Pampa del Tamarugal; C, Calama; SdA, Salar de Atacama; pAb, pre-Andean basins in general). The shade of gray shows the relative steepness of the long-wavelength west facing slope, from light gray (inclined ~1–2°) to darker gray (inclined 3–4°). Superimposed on both the long wavelength sloping planes and on the subhorizontal (white) platforms is a complex, subdued, landscape of the Mesozoic through Eocene mountain ranges (not shown).

presented here, based on a completely independent approach, show an uplift history that is coherent with the *Hoke et al.* [2007] results, with improved age resolution.

3. Morphology and Structure of the Western Andean Slope

[12] The Western Andean Slope is the region that has undergone the topographic change that created the western margin of the Andes. We define the mountain front(s) in the region between the Western Cordillera and the Pacific Ocean (for our northern study area) or the Central Depression (for the Salar de Atacama basin) as being regions with average west facing slope in excess of 1.5°. We generated the slope of average topography (Figure 3a) from the SRTM 90 m data using a 21 km × 21 km moving window average, a window that exceeds the size of the high-frequency topographic elements yet is smaller than the large-scale tectonic landform that we wish to isolate [*Hoke*, 2006]. North of 22°S, these slopes reveal a very simple structure to the Andean mountain front (Figures 3a and 3b), with a single relatively narrow belt in which slopes are inclined 3–5° to the west, which connects the fore-arc basins of northern Chile and southern Peru to the Altiplano plateau. We call this simple plane, inclined 3–5°, the Western Andean Slope [*Isacks*, 1988; *Hoke*, 2006; *Hoke et al.*, 2007]. South of 24°30′S there is also a single strand to the Western Andean Slope, albeit with a form that is more complex than it is north of 22°S. Between 22°S and 24°30′S the slope map pattern is more complex, with two north trending zones in which the west facing slope (21 × 21 km average) exceeds 1.5° (Figures 3a and 3c). Here there is an eastern narrow, steep plane (3–5° slope) which is the ultimate topographic step to the Puna plateau and which we identify as the principal Western Andean Slope. But there is also a diffuse, complex mountain front farther west in the fore arc, defined by slopes of ~1.5°–3°, which seems to be a western branch of the Western Andean Slope.

[13] Adjacent to the Altiplano, the nonmarine fore arc is narrow; the distance from Pacific Ocean shoreline to the western rim of the Altiplano is ~110 km (Figures 2 and 3). The single-strand Western Andean Slope is ~50 km wide and 3000 m in relief, from the lowlands of the Central Depression at ~800–1000 m above sea level on its western side to the Altiplano plateau on its eastern side. Here the Central Depression and lower Western Andean Slope host the Pampa del Tamarugal fore-arc sedimentary basin. Adjacent to the northern Puna plateau (22–25°S), the fore arc is much wider, ~200–250 km, quite irregular, with a western Central Depression that does not presently collect a significant volume of sediments and thus is not today a fore-arc basin. Here, the Calama and Salar de Atacama basins, the northern two of a set of basins termed the Pre-Andean basins, occur in the eastern fore arc and stand above 2300 m altitude. The east branch of the Western Andean Slope is the eastern topographic feature in the fore arc. It is ~25 km wide by 2000 m high, and uncommonly steep (5°) (Figures 3a, 3c, and 4) [*Hoke*, 2006]. Seismological data have shown that the crust and upper mantle beneath the Salar de Atacama and Calama Pre-Andean basins are uncommonly cold and strong, producing what *Schurr and Rietbrock* [2004] referred to as the Atacama block (Figure 2).

[14] Although not recognized in most mountain belts as a structural style related to important relief development, monoclinal folds [e.g., *Davis and Reynolds*, 1994] with west facing limbs are the most common Neogene structural style of the Western Andean Slope. Prior studies demonstrated that both west vergent short-wavelength [*Muñoz and Charrier*, 1996; *Victor et al.*, 2004; *Pinto et al.*, 2004; *García and Hérail*, 2005; *Farías et al.*, 2005; *Muñoz*, 2007] and long-wavelength monoclines [*Isacks*, 1988; *Farías et al.*, 2005; *Hoke et al.*, 2007; *Schildgen et al.*, 2007, 2009b] contributed to development of topographic relief across the Western Andean Slope. Although the magnitude and history of vertical displacement across short-wavelength monoclines have been demonstrated largely north of 20°S, *Victor et al.* [2004] and our new field and seismic mapping demonstrate that similar features persist to 21°30′S (Figure 2). The long-wavelength monoclinal shaping of the Western Andean Slope has been pronounced since ~10 Ma (Figure 5) [*Farías et al.*, 2005; *Hoke et al.*, 2007; *Schildgen et al.*, 2007, 2009a].

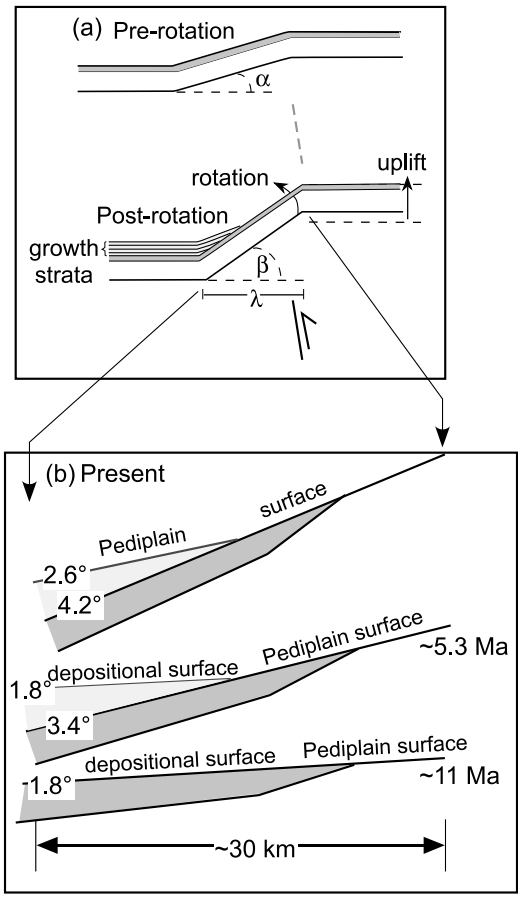

Figure 5. (a) Geometric components of a schematic monocline fold [after *Patton*, 2004]. The dark gray unit indicates pre-growth strata, whereas light gray are strata that accumulate contemporaneous with growth of structural relief. Topographic relief in the top cross section is the consequence of events that pre-date the monocline. (b) Progressive steps in deposition and tectonic rotation of the long-wavelength monocline at the eastern margin of the Pampa del Tamarugal basin, based on data in Tables 1a–1c. The dark gray polygons (AdP) accumulated during the early and middle Miocene, contemporaneous with structural relief growth across small-scale folds but pre-growth relative to growth of relief across the large-scale (~30 km limb width) monocline. The light gray form represents the Arcas unit.

[15] We estimate the rise of the southern Altiplano, northern Puna, and adjacent Western Andean Slope (Figure 4) through time using the strata that fill the lowland fore-arc basins (Figure 2). To accomplish this we measure at multiple time steps the magnitude of newly created structural relief from a position within the basin to a position part way to the crestline of its catchment area on the Western Andean Slope for stratigraphic surfaces of known age in three basins, the Pampa del Tamarugal, Salar de Atacama, and Calama basins (Figures 2 and 4). While our data only directly measure the monocline evolution for the lower part of the Western Andean Slope (the range of elevations covered by fore-arc basin strata), the simplicity of the monoclinal landform allows us to extrapolate the result to the rim of the plateau at higher elevation.

4. Conceptual Framework

[16] As pointed out by *England and Molnar* [1990], it is important to distinguish between surface uplift, rock uplift, and exhumation, where surface uplift equals rock uplift minus exhumation–our objective is to measure surface uplift. Because erosion is extraordinarily slow in the hyper-arid Atacama Desert, with values less than 1 m/Myr having been measured by a variety of techniques [*Kober et al.*, 2007; *Dunai et al.*, 2005; *Ewing et al.*, 2006; *Hoke*, 2006; *Carrizo et al.*, 2008; *Evenstar et al.*, 2009], exhumation has been negligible during the late Miocene to Holocene, except in the canyons of southern Peru and northernmost Chile [*Hoke et al.*, 2004; *García and Hérail*, 2005; *Schlunegger et al.*, 2006; *Thouret et al.*, 2007; *Schildgen et al.*, 2007, 2009a; *Kober et al.*, 2007]. Consequently, for the area between 20°S and 24°S that lacks deep canyons, rock uplift effectively equals surface uplift.

[17] To study uplift or subsidence, a frame of reference must be specified in which to measure displacement relative to an equipotential surface of gravity, such as the geoid. The geoid is approximated by mean sea level and so to measure uplift and subsidence, paleoaltitude information is needed, such as that obtained in proxy studies [*Charrier et al.*, 1994; *Gregory-Wodzicki*, 2000, 2002; *Ghosh et al.*, 2006; *Garzione et al.*, 2006, 2008]. In studies measuring relief generation, such as the current study, the measurements determined can only be converted to absolute uplift and subsidence values if the elevation history of some reference level within the system is known. Because the strata studied lack a direct association with a paleo-elevation datum, our direct results are a history of relief development.

[18] From the perspective of a sedimentary basin, the relief generation that we wish to measure is the increase of topographic relief through time of the basin's catchment area, a sum of uplift in the headwaters and subsidence in the basin. Specific to this study, the structural relief is the sum of absolute subsidence, if any, of the fore-arc basin and absolute uplift of the Altiplano-Puna plateau. The topographic relief may be less than the structural relief because the lowland areas fill with sediments. Since we wish to examine the uplift history of the Altiplano-Puna plateau surface independently of paleoaltitude estimates from proxy data, we must estimate the contribution of tectonic, isostatic, and compaction subsidence in the basin end of the areas studied if we are to extract from the structural relief data the surface uplift of the plateau flank. Fore-arc sedimentary basins have no standard for tectonic subsidence: some subside by thousands of meters, others do not subside at all [*Dickinson*, 1995]. The northern Chilean fore arc is constructed on continental lithosphere, which tends to minimize fore-arc tectonic subsidence [*Dickinson*, 1995], although large magnitude tectonic subsidence occurs in the marine fore arc farther west [*von Huene and Scholl*, 1991; *von Huene et al.*, 1999; *von Huene and Ranero*, 2003; *Sick et al.*, 2006].

[19] In any nonmarine sedimentary basin there are two alternatives that may explain the potential to accumulate sediments: tectonic subsidence, or inherited closed topographic lows that were generated during earlier tectonic episodes. Tectonic subsidence is commonly associated with large-offset faults, which drive contraction or extension that in turn controls the topographic loading and the accommodation geometry at a large scale [e.g., *Jordan*, 1981]. Syn-orogenic strata and syn-depositional structures are common features in tectonically subsiding basins [e.g., *Riba*, 1976; *DeCelles et al.*, 1991]. In contrast, sub-horizontal strata across the width of a basin with only modest thickness of strata, laterally abrupt stratal termination by onlap onto an older basement, a lack of faulted margins, and a lack of large-offset faults within the basin are good indications that there was little or no tectonic subsidence and that sediment ponded in a topographically closed valley. Whether the space in which to accumulate sediment is provided by tectonic subsidence or by inheritance of a topographic low, the magnitude of that underlying control is amplified by isostatic subsidence and compaction subsidence.

[20] At a regional scale (Figure 2), the northern Chilean fore-arc records several hundred meters of Oligocene and younger sediment [*Nester*, 2008; *Charrier et al.*, 2007; *Nester and Jordan*, 2010] which, by the standards of sedimentary basins, is a small accumulation [*Busby and Ingersoll*, 1995]. The Pampa del Tamarugal basin, for example, is broad and thin and reflects little or no tectonic subsidence. In contrast, the Salar de Atacama basin [*Muñoz et al.*, 2002; *Arriagada et al.*, 2006; *Jordan et al.*, 2007] has thousands of meters thickness of Neogene strata, locally showing rotational syntectonic features. Such thick accumulations require an explanation of the accommodation space.

[21] In the following we refer to structural relief when presenting our measurements based on the long-wavelength kinematic displacement of stratigraphic surfaces. At the end of the paper we examine the evidence for subsidence in the fore-arc basins and what this signifies for surface uplift estimates of the plateau derived from our structural relief data.

5. Methods to Quantify Monoclinal Structural Relief Formation in the Fore-Arc Basins

[22] We pick stratigraphic markers that occur along the eastern flank of the fore-arc basin and whose depositional age and environment have been studied in surface exposures. Selected marker horizons were projected, or in some cases traced, into the subsurface, where they can be traced for many kilometers using the seismic data. Following structural criteria and by inspection of depth sections (Figure 6), we also defined the location within the basin of the western limit of the long-wavelength rotation (lower hinge, Figure 5). A key criteria for selecting profiles across the basins and western slope is that, at the eastern extremes of the basin, local-scale blind or emergent faults do not separate the lowland strata from the Western Andean slope.

5.1. Data

[23] On a grid of 2D seismic reflection data we map the spatial extent of the dated horizons. Where exposures permit, we either compile existing geologic maps, or we map on the ground and using remote sensing the spatial extent of Neogene units, especially those that prove to be resolvable in the seismic data. The suitable seismic profiles are converted to depth using seismic velocity information available from scarce boreholes and extensive stacking velocities. Geologic cross sections (e.g., Figure 6) are created from these depth data and surface exposures of the same units.

5.2. Estimation of Rotation and Uplift

[24] The differences between the inclinations of the modern topographic slope and the inclinations of successive paleoslopes are calculated. After certain corrections (described below), the angular differences between the successive inclinations (Figure 5, $\beta - \alpha$) represent the amount of long-wavelength rotation that occurred during the times spanned between those successive surfaces. By linear extrapolation we extend the rotation thus estimated for the Western Andean Slope to the position of the upper hinge of the monocline to calculate by simple geometry (Figure 5, $\beta - \alpha$ and λ fully describe a triangle) the structural relief that was generated by that rotation. This estimate of structural relief growth is inclusive of all deformation mechanisms that might in concert produce the crustal deformation that underpins the long-wavelength monocline.

[25] Corrections take into account the primary depositional inclinations of all surfaces, and under certain circumstances corrections are needed for rotation due to compaction (Supplementary Data). The primary depositional inclination is estimated from the depositional facies of the strata whose ages are known, by analogy to modern depositional systems with similar deposits in the same modern basin. For groundwater fed evaporites or lacustrine deposits, the modern environments have a horizontal starting condition. For alluvial deposits, the depositional slope is controlled by sediment textures and hydrology [e.g., *Paola and Mohrig*, 1996], which are driven by catchment basin bedrock characteristics and by climate. For cases in which the modern day alluvial fans emanate from the same catchments as did the Miocene and Pliocene alluvial fans, we here assume that surface inclinations of active alluvial fans approximate the depositional inclinations of the alluvial strata, recognizing that paleoclimate variability and catchment evolution introduce uncertainties. For alluvial deposits, we determined the surface slope of the modern alluvial fan apices, located by visual inspection of Landsat TM images; slopes were quantified with DEMs (90 m shuttle radar topography mission [SRTM] data) of the ephemeral stream channels on the fans. Only stream channels that lack obvious recent fault or fold perturbations near their transition from erosional to aggradational at the canyon mouths were considered. Longitudinal channel profiles were created using the 90 m SRTM data, with a vertical resolution of a few meters, and depositional slopes were determined for positions bounded to the east by the point of unconfined flow, and to the west

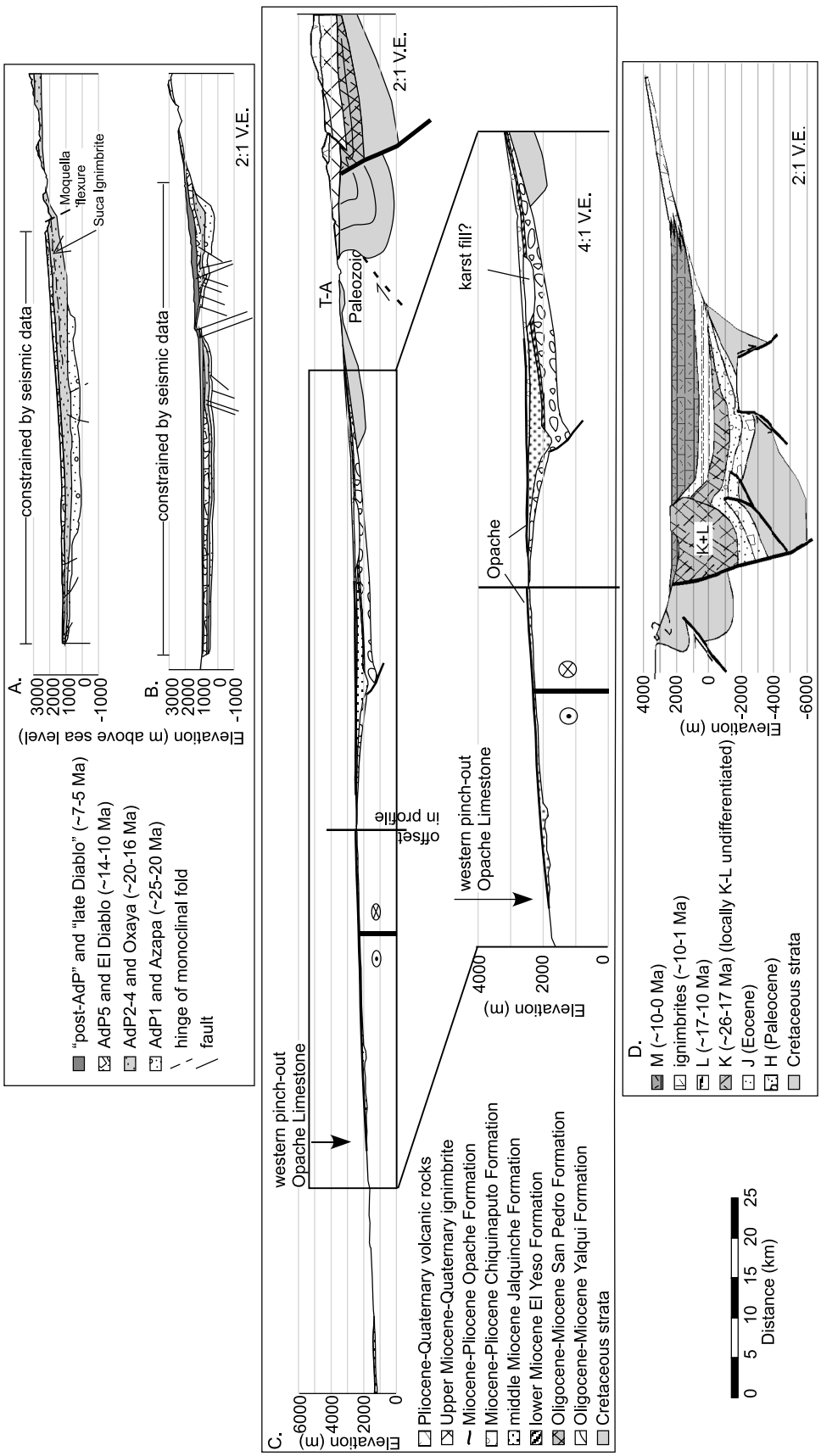

Figure 6. Cross sections showing key stratigraphic units in the Cenozoic strata of the fore-arc basins, principal folds and faults, and long-wavelength tilting (see Figure 2 for lines of section). All are plotted with 2:1 vertical exaggeration, with an inset in Figure 6c at 4× vertical exaggeration. (a and b) Pampa del Tamarugal, (c) Calama basin (T-A marks the Tuina-Aiquina ridge), (d) Salar de Atacama basin.

by the location 3 km downslope from the point of unconfined flow. This starting condition is considered to be the greatest depositional slope for the alluvial fan system and thus would lead to minimization of the perceived post-depositional rotation.

[26] If the thickness or dominant lithology of strata underlying a horizon of interest or the thickness of strata burying a horizon of interest changes along our profile of interest, differential compaction of strata beneath the horizon of interest may lead to gentle tilting. We estimate the progressive compaction of multiple points along the profiles of interest using sparse data, numerical approaches developed in other sedimentary basins [*Sclater and Christie*, 1980], and the software developed by N. Cardozo (OSX-Backstrip. http://homepage.mac.com/nfcd/work/programs.html). We employed a range of possible parameter values to test the uncertainty in the compaction, calculated the corresponding compaction-tilting, and removed the compaction-tilting from the observed inclination (detailed in the auxiliary material).[1]

5.3. Positions of Monoclinal Hinges

[27] The western limit of the long-wavelength rotation is located by visual inspection of seismic reflections on the available seismic lines. The hinge is identified as the position of the break-in-slope from an eastern zone with a comparatively large magnitude westward inclination to a western zone of more nearly horizontal layers. We define the eastern limit of the long-wavelength monoclinal rotation as the set of points where swath topographic profiles indicate topographic rollover, from a western zone with a low-relief landscape surface that averages ~4.0° west dip, to an eastern sub-horizontal and more irregular surface. The west-to-east swath profiles are constructed from the 90 m SRTM digital topography. The position of the rollover between the plateau and the Western Andean Slope was identified on each swath and transferred to a base map (e.g., Figure 7).

5.4. Uncertainties

[28] The sources of uncertainty on quantification of relief formation from long-wavelength rotated strata include (1) Consistency in the identification in the field and in seismic profiles of the stratigraphic markers. (2) Conversion of seismic reflections measured in two-way travel time (TWT) to depth using sparse seismic velocity data. (3) Non-uniqueness of the model of compaction of underlying units. (4) Structural interpretation, which requires that we correctly identify parts of seismic lines that display long-wavelength monoclinal tilt rather than rotation across local-scale faults or folds. (5) Uncertainties of primary depositional slopes. Uncertainties are quantified from the variability of data among multiple cross sections considered, estimated from models in the case of compaction and conversion of seismic time sections to depth sections, and reported but not quantified from other sources, such as inadequacies in data, observations, and theory. We make two assumptions about the errors in measurements of a variety of parameters, that they are independent and that the error on each type of measurement is governed by a normal distribution. In the case of derivative quantities calculated by summing or subtracting constituent values, we report the uncertainty on the derivative quantity to be the square root of the sum of the squares of the standard deviations of the constituent values. In the case of derivative quantities calculated by multiplication or performing trigonometry, we propagate the fractional uncertainties [*Taylor*, 1997].

[29] Where our new mapping is incorporated (i.e., Pampa del Tamarugal basin, Calama basin), the uncertainty on the inclinations of the paleosurfaces in outcrop results from the uncertainties on our recognition of the chronostratigraphic units, and error in the topographic data. The mapping is based on months of field observations by senior field geologists and by a suite of ash ages [*Blanco*; 2008; *Nester*, 2008] (Table S1 in the auxiliary material), but the uncertainty of our stratigraphic mapping is unknowable. Analyses of error on the Shuttle Radar Mission Topography (SRTM) 1-arc-second data by *Castel and Oettli* [2008] and *Falorni et al.* [2005] reveal vertical errors of <20 m.

[30] The conversion of seismic travel time to depth to any given reflector within the Neogene deposits is uncertain because there are insufficient sonic velocity logs available for the lithofacies in the eastern part of any of the basins. The alternative, to estimate sonic velocities from stacking velocities, is at best approximate. Errors introduced by these methods are systematic rather than random.

[31] Because the position of the upper rollover of the monocline is chosen based on topographic form even though it occurs at high elevations where the climate is comparatively wet (arid to semi-arid) and thus suited to denudation of the monoclinal surface, there is the possibility that we underestimate the width of the monocline. This potential under-estimation of λ means that our result for the relief growth of the western margin of the Central Andean Plateau is more likely to be an under-estimate than an over-estimate.

[32] Chronological information specific to a given sample is reported with 2-sigma laboratory errors when the primary information source specified the nature of the uncertainty (details in Table S1).

6. Description and Analysis of the Pampa del Tamarugal basin (19°–22°S)

6.1. Landforms and Surface Processes

[33] The Pampa del Tamarugal (PdT) in northern Chile is a narrow (~50 km), elongate (~400 km), north trending fore-arc sedimentary basin whose axis is ~1000 m above sea level. The basin lies east of, and onlaps, a narrow Coastal Cordillera, which attains elevations of between ~1000 and 2000 m at the latitudes of interest to this study. To the basin's east the Western Andean Slope rises steadily, with long-wavelength surface inclinations that progressively change from a 2° to 3° west dip at the toe of the slope to an upper sector that averages 4–5° (Figure 3) [*Hoke*, 2006]. The altitude of the eastern hinge of the Western Andean Slope is ~4000 m (Figures 2 and 3). Narrow but deep west

[1] Auxiliary materials are available in the HTML. doi:10.1029/2010TC002661.

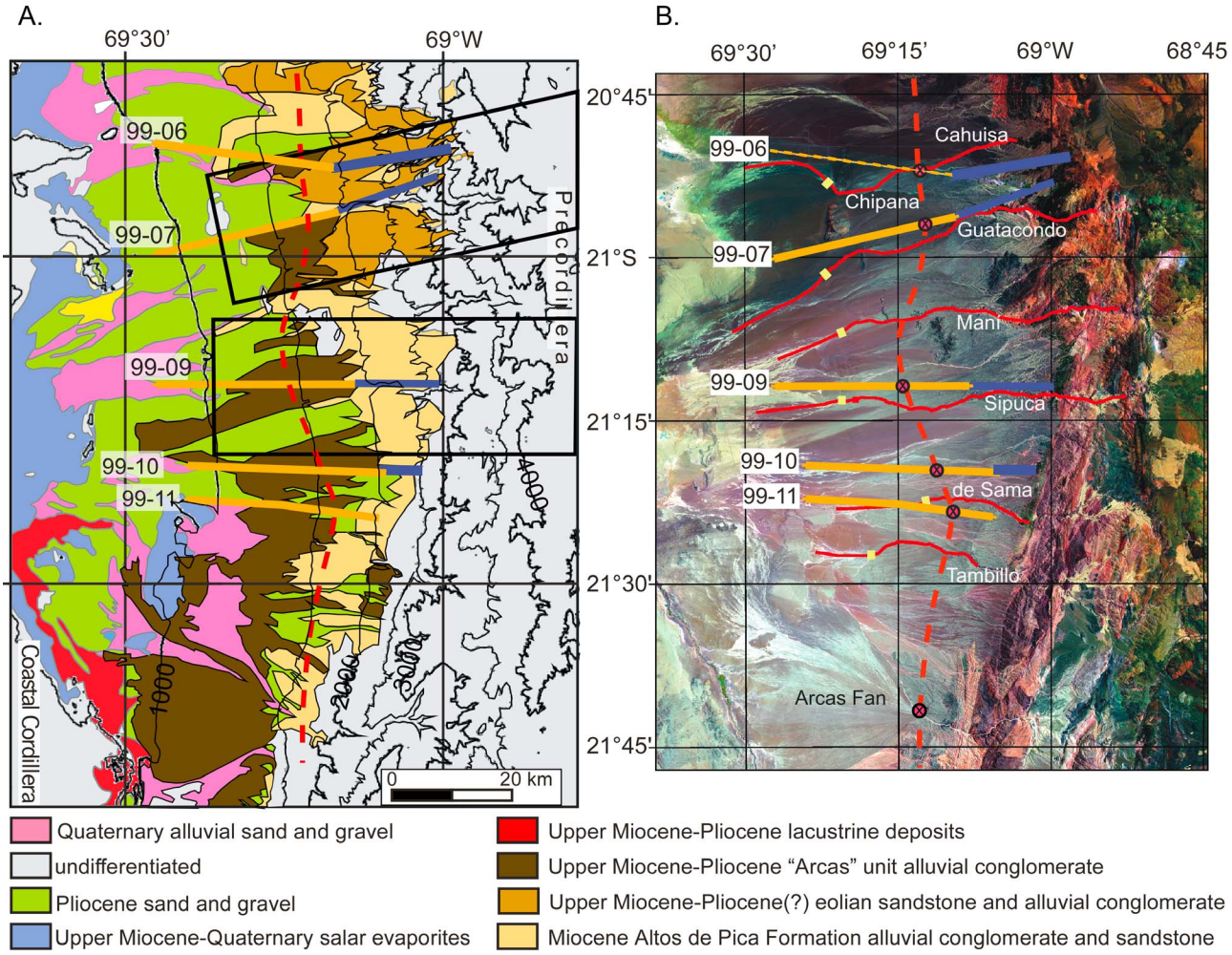

Figure 7. (a) Simplified geologic map of the southern Pampa del Tamarugal with topographic contours (CI = 500 m). Orange lines mark the positions of seismic reflection profiles reported here; the thick blue lines span a pair of parallel topographic transects along which geologic cross sections were constructed to the east of the seismic data (Figure 8). The dashed red line represents the approximate downdip hinge of the monoclinal fold, identified along individual profiles at a cross within a circle. The two trapezoids mark 20-km-wide swaths in which topographic profiles define the roll-over at the updip hinge of the monoclinal fold [*Nester*, 2008]. (b) Landsat TM image of the study area, illustrating the locations of modern channels used in the study. Red lines indicate the locations of channel profiles detailed in Figure 8, and the yellow tick marks along their courses indicate the point at which the channels transition from confined (upstream, east) to unconfined (downstream, west). Crosses represent locations of monoclinal fold axes based on seismic profiles (lines 99-06, 99-07, 99-09, and 99-10), the eastern limit of horizontal strata (line 99-11), and the lack of rotation of the Arcas Fan, and from these the dashed red line is drawn as a generalization of the western hinge position. Orange lines as in Figure 7a. Blue lines mark the general position of the geologic profiles east of the seismic lines. The location of the fossil, latest Miocene Arcas Fan in the southern part of the basin is noted [*Kiefer et al.*, 1997].

trending canyons, typically spaced 10–20 km apart, are the most significant short-wavelength relief. Between the canyons exist broad, low-relief, surfaces that at a long wavelength dip gently to the west (<2°), the pediplains (Figure 3). The results are that the most extensive landform seen on an east-west cross section is a gently concave pediplain. North of ~19°45′S, the principal canyons are very deeply incised (2–5 km wide, ≤1000 m deep) and drain to the Pacific Ocean. Farther south, in contrast, canyons are only incised within the Western Andean Slope and the proximal sector of the basin (1–2 km wide, 10s to 100s of m deep), adjusted to a local base level set by the surface of the Pampa del Tamarugal basin.

[34] The rocks on which the inter-canyon pediplain is constructed differ from the western, lower elevations to the eastern, higher elevations (Figures 6a, 6b, and 7). This

lithologic boundary generally occurs in the range of 2500 to 3000 m altitude. At higher elevations, deeply eroded Paleozoic and Mesozoic rocks and laterally extensive Oligocene-Miocene volcanic rocks underlie the pediplain and western Andean slope. At lower elevations, the pediplain and lower part of the western Andean slope are underlain by Oligocene-Miocene fore-arc basin strata, the focus of this paper. North of ~19°45′S where canyons drain to the Pacific Ocean, the fore-arc basin does not currently trap sediment. At latitudes south of 19°45′S at elevations below ~1200 m, the basin still accumulates both siliciclastic and evaporite deposits when the climate conditions result in transport of weathering products to the basin (Figure 7). North of ~20°S the basin fill is highly continuous with very few faults or folds except at its western boundary with the Coastal Cordillera (Figure 6a), whereas the southern part of the basin is widely disrupted by meter- to hundred-meter-scale reverse and normal faults [*Nester*, 2008] (Figure 6b).

[35] In the fore-arc basin, nearly all of the siliciclastic sediments accumulated in broad alluvial fans whose apices are near the eastern margin of the PdT basin and whose distal toes nearly reach the Coastal Cordillera (Figure 7). At the western edge of the PdT a discontinuous chain of salt pans (salars) form in lows, which under wetter climates would result in a series of lakes. Between 20°S and 22°S, the focus of this study, modern siliciclastic detritus is transported into the basin infrequently as sheet floods, mudflows and debris flows [*Houston*, 2002; *Kiefer et al.*, 1997], and often retransported by wind. Throughout the Pampa del Tamarugal and Coastal Cordillera of northernmost Chile the climate is hyperarid, whereas at elevations above 3500 m the highlands of the Western Andean Slope and Altiplano are arid to semiarid. The landform consequences are that small masses of siliciclastic debris, chemical solutes, and water are delivered to the lowland basin, but the erosion of the pediplain landscape is so slow that over millions of years there has been only several meters of degradation [e.g., *Kober et al.*, 2007]. On centennial to millennial scales, intervals of increased precipitation in the highlands resulted in increased activity of streams in the canyons that deliver sediment to the basin, and resulted in slight channel erosion on the pediplains [*Nester et al.*, 2007; *Evenstar et al.*, 2009].

6.2. Stratigraphy

[36] Prior studies [e.g., *Pinto et al.*, 2004; *Farías et al.*, 2005; *Hoke et al.*, 2007; *Nester*, 2008] reveal that the Oligocene and Neogene stratigraphy of the PdT is dominated by nonmarine siliciclastic deposits accumulated in alluvial, lacustrine and eolian environments, evaporites formed in salt pan environments, and ignimbrites produced by pyroclastic flows. As well documented in the literature, the Oligocene and Miocene strata north of ~19°30′S constitute a succession of formations (base to top, Azapa, Oxaya, and El Diablo) [e.g., *Pinto et al.*, 2004; *Farías et al.*, 2005]. In eastern parts of the northern basin, the top of the El Diablo Formation is no younger than ~9 Ma [*Pinto et al.*, 2004] and an unconformity tops the El Diablo Formation, across which there is a time gap of ~9 Myr. The duration of this hiatus diminishes toward the west [*von Rotz et al.*, 2005]. The Altos de Pica Formation (AdP) south of 19°30′S formed during much of the early and middle Miocene. In eastern parts of the southern basin, the AdP's top is ~11 Ma to ~12 Ma (Table S1). In eastern sectors of the basin, an unconformity tops the AdP and El Diablo Formations, across which there is a time gap of ~5 Myr (in much of the southern region) to ~9 Myr (in the north). The duration of this hiatus diminishes toward the west.

[37] We focus in the southern part of the basin, 20°–22°S, where the Oligocene and Neogene strata of the eastern part of the basin consist, from base to top, of the Altos de Pica Formation (AdP) and a series of upper Miocene to Pliocene strata that lack formal stratigraphic names (Figure 7). The AdP has been subdivided into members 1–5 based on lithologic variations observed in outcrop at ~20°30′S [*Dingman and Galli-Olivier*, 1965]. Sandstones of eolian and fluvial origin are common in the northern part of the study area, with less abundant fluvial conglomerate interbeds, whereas debris flow and fluvial conglomerates dominate in the southern part of the study area. Based on the coarse alluvial facies of the AdP at the eastern margin of the basin, the eastern limit of preserved strata may approximate the location of the Miocene depositional pinch out. This eastern limit occurs at elevations ranging from as high as 3600 m in the north, to only ~2200 m in the far south (Figure 7). Ages of all members of the Altos de Pica Formation are constrained by dates on intercalated ashes, ignimbrites, and conglomerate clasts of volcanic origin (Table S1). The youngest dated horizons near the top of the unit are of late middle Miocene age, yet the youngest horizons might be as young as the very earliest late Miocene, ~11 Ma (Text S1, section S1.1).

[38] Along much of the eastern fringe of the basin, the AdP was followed by a long hiatus (Figure 7). Over wide sectors of the basin, the AdP is unconformably overlain by poorly consolidated upper Miocene eolian and alluvial deposits (see Text S1, section S1.1). Upper Miocene-Pliocene alluvial deposits are typified by the relict Arcas mega-fan in the south (Figure 7) [*Kiefer et al.*, 1997], which include a latest Miocene ignimbrite interbed [*Hoke et al.*, 2007] (Table S1). An onlap relation between the westward dipping top of AdP and the Arcas unit is exposed in the upland part of the Western Andean Slope where the Arcas fills broad canyons that were incised into the upper member of the AdP, as well as in the lowland subsurface where seismic data reveal onlap geometries [*Nester*, 2008]. However, the Arcas unit was short-lived, estimated by *Kiefer et al.* [1997] to encompass less than a million years. Over broad regions south of 21°15′S (Figure 7), above the Arcas unit the regional expression of the last 5 Myr is a hiatus. North of that latitude, Pliocene and Quaternary alluvial fan landforms are widespread west of the monocline.

[39] In the western part of the basin, deposition was more continuous during the late Miocene and Pliocene than in the eastern basin. North of 20°S, upper Miocene alluvial siliciclastic and lacustrine diatomite units are considered to be a western facies of the El Diablo Formation [*von Rotz et al.*, 2005], which suggests a westward offlap of deposition. These are capped by undated salt pan evaporites. Canyon incision had begun by 6.4 Ma [*Kober et al.*, 2006; *Hoke et al.*, 2007] but did not approach the extreme magnitude seen today until younger than 5.5 ± 0.6 Ma [*Naranjo and*

Paskoff, 1985] or younger than 3.49 ± 0.04 Ma [*Allmendinger et al.*, 2005]. In the south, the western toes of the Arcas alluvial fans are overlain by lacustrine upper Miocene-Pliocene limestone, diatomite, and evaporite [*Sáez et al.*, 1999].

[40] For this study, the most important attribute of the Miocene and Pliocene depositional environments is the primary depositional slope, which set the original geometry of the strata, and the most direct means to estimate the primary depositional slope is by comparison to modern landforms. Because the depositional slope is controlled by sediment textures and hydrology [e.g., *Paola and Mohrig*, 1996], we need to consider whether the catchment geology and the paleoclimate during the middle Miocene through Pliocene were like those that control the modern alluvial fans. The catchment geology of the southern Pampa del Tamarugal has changed little since deposition of the youngest member of the AdP because the catchments do not reach into the volcanic arc. For example, in one of the largest catchments (>700 km^2) of the study area, *Kiefer et al.* [1997] demonstrate down-cutting of ~160 m averaged across the catchment of the Arcas Fan since about 7 Ma, a small magnitude that would not have markedly altered the bedrock geology of the catchment. Since late in the middle Miocene the mean climate condition in the study area has been hyperarid, as it is today [*Rech et al.*, 2009], though times of slightly enhanced precipitation were most likely associated with the times of greatest erosion and deposition [e.g., *Nester et al.*, 2007] and thus with the paleohydrology of the times of alluvial accumulation. The only direct proxy available for the paleo-hydrology is the sedimentary fabric. In the southern PdT, our focus area, the depositional texture and fabric of modern alluvial deposits are similar to those of the upper member of the AdP and to some parts of the Arcas unit. The strata of AdP member 5 are an intercalated mixture of poorly sorted, tabular, matrix-supported gravels, and poorly sorted, tabular, gravelly muds. The Arcas unit possesses intervals of fabrics like those in AdP member 5, as well as intervals of moderately sorted, clast-supported gravels with local horizons that are weakly imbricated and moderately well sorted. Surficial deposits comprised of debris flows and mudflow sheets with fabrics like those in AdP member 5 extend many kilometers across the Pampa, generated during infrequent sheet floods and sediment-gravity flows [*Houston*, 2002]. In sum, we interpret that catchments, paleoclimate and environments during these three time intervals were similar and that their primary depositional slopes were similar.

6.3. Data

[41] The subsurface stratigraphy and structure of the Pampa del Tamarugal valley was mapped using 14 reflection seismic lines, logs and cuttings from 4 hydrocarbon exploration boreholes, and sedimentological and chronological data from surface exposures (Figure 7) [*Nester*, 2008]. Since only 2 wells directly tie to seismic data, we relied extensively on surface geology along the traces of the seismic lines to tie surface stratigraphy to seismic stratigraphy, especially the locations where reflectors intersect with the land surface. Four of the east-west oriented seismic lines, reported here, between 20°50′S and 21°20′S (99-06, 99-07, 99-09 and 99-10) image the transition from the valley to the Western Andean Slope where there are no local faults that cut the AdP or Arcas units. The modern dips of top horizons of the AdP member 5 and of the upper Miocene-earliest Pliocene strata were calculated from depth-converted cross sections based on the seismic reflection profiles and from surface exposures of strata (Tables 1a–1c and Figures 7 and 8).

[42] Cenozoic units were mapped in the field and on a Google Earth image base, and the positions of unit contacts were transferred to depth sections (Figures 7 and 8). Depth profiles of the top of AdP based on the seismic data were connected to profiles of the altitudes of the tops of the AdP and of the Arcas unit in outcrop, and continued to their updip limits (Figure 8).

[43] For the upper portion of the Western Andean Slope, east of the updip exposure limit of the AdP and Arcas units, the area north of 21°30′S is largely free of local-scale faults and folds with activity younger than 10 Ma (Figure 2) [*Victor et al.*, 2004; *Tomlinson et al.*, 2001]. The adjacent plateau margin contains numerous normal, strike-slip and reverse faults younger than 10 Ma, but displacements typically are no more than 10`s of meters [*Tomlinson et al.*, 2001; *Victor et al.*, 2004]. Between 21°30′S and 22°S a steeply west dipping, east vergent reverse fault, the Arcas Fault, lies immediately east of the Western Andean Slope (Figure 2) [*Tomlinson et al.*, 2001; *Blanco and Tomlinson*, 2006]. It may have contributed to some long-wavelength westward tilting along the Western Andean Slope, via back-tilting in its hanging wall block, but offsets of the Altos de Pica Formation along the fault are only on the order of 50–200 m, and the fault displacement diminishes to the north, being negligible at the latitude of the seismic-geologic profiles used here.

[44] A geometrical starting condition for the depositional surfaces is estimated through analogy to the depositional angles of the proximal sectors of modern and currently aggrading alluvial fan surfaces in the same area. For stream channels that meet the criteria that they lack evidence on Landsat TM images, a Digital Elevation Model (DEM), and seismic profiles of recent fault or fold perturbations near their transition from erosional to aggradational behavior (e.g., Cahuita-Chipana, Guatacondo, Maní, Sipuca, de Sama and Tambillo drainages), longitudinal channel profiles were extracted from the DEM over distances of ~25–30 km (paths of profiles shown on Figure 7, and the profiles on Figure 9). We focus on the average inclination of the most proximal 3-km-wide reach of the aggradational zone, bounded on the east by the position of transition from confined to unconfined flow (Figure 9 and Tables 1a–1c).

[45] The location of the western limit of slope rotation was mapped for seismic lines 99–06, 99–07, 99–09, 99–10 where inclination of the top of the AdP decreases westward (Figure 8). The ability to distinguish between instantaneous limb rotation and progressive limb rotation would be ideal [*Suppe et al.*, 1992], however the seismic data do not resolve the internal geometry of the Arcas unit. Just as revealing are

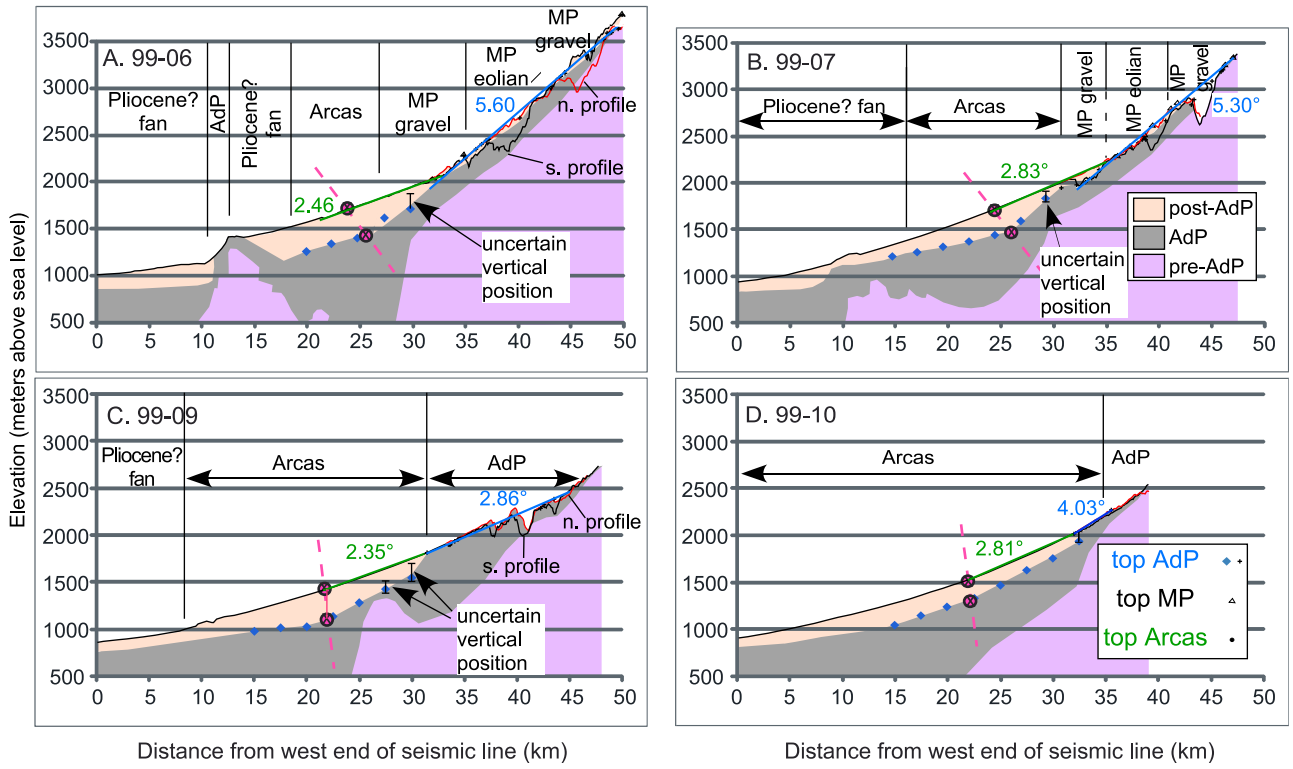

Figure 8. Positions of paleo-surfaces used to determine angles of rotation for 11 and ~5 Ma time periods along and to the east of seismic lines 99-06, 99-07, 99-09 and 99-10. The blue diamonds (from seismic data) and pluses represent the upper surface of the Altos de Pica Formation (AdP); the triangles represent the upper surface of the upper Miocene-Pliocene eolian and alluvial deposits (MP) in the northeastern region; the circles mark the top of the Arcas unit in outcrop and except as noted, the Arcas unit is the top surface of the lowlands in the western part of each profile. The subsurface positions of the top of the Altos de Pica member 5 (blue diamonds) derived by converting reflectors from time to depth using interval velocities at 2.5 km intervals (100 shot points). For each cross section east of the seismic profiles, two parallel topographic profiles are shown, one black and one red, spaced <1.5 km apart. Crosses in red circles represent a change in angle of the paleo-surfaces, and the red dashed line indicates the interpreted location of the western limit of rotation. The surface geologic unit traversed by the line of section is labeled. A green line segment approximates the upper surface of the Arcas unit between the monoclinal hinge and the Arcas pinch out; its inclination is indicated in green numerals. A blue line segment approximates the upper surface of the Altos de Pica Formation; its inclination is indicated in blue numerals.

topographic profiles with no evidence for post-late Miocene rotation, such as across the late Miocene–early Pliocene Arcas Fan (at the latitude of 21°42′S) where, west of the fossil fan apex, there was no tectonic rotation younger than ~5 Ma [*Nester*, 2008]. By inference, the western limit of surface rotation lies east of the apex of the Arcas Fan. Horizontal reflections in another seismic line, 99–11, constrain any rotation younger than ~15 Ma to a position east of 69°10′W. The eastern hinge of the monocline was located on two west-to-east swath topographic profiles (Figure 7) [*Nester*, 2008] and transferred to a base map.

[46] Although differential compaction would have caused rotation to the west of the AdP under the weight of the Arcas unit, the small thickness of the Arcas unit (≤320 m in the area where the seismic data record the long wavelength rotation) minimizes the compaction rotation (Text S1, section S1.2).

6.4. Pampa del Tamarugal Results

[47] Depositional angles for proximal modern unconfined alluvial sediments along six channels were documented (Figures 7 and 8), and the most proximal 3 km of each averages 1.8 ± 0.2°, with a range between 1.6° and 2.0° (Tables 1a–1c). This is in the transitional realm from alluvial fan sediments [*Blair and McPherson*, 1994] to larger distributive fluvial systems [*Hartley et al.*, 2010]. This angle, 1.8° ± 0.2°, is taken as the original proximal fan depositional angle for all alluvial sediments in the Pampa del Tamarugal Basin. Because this mean represents the most proximal and steepest section of each fan system, we consider that this assumed primary dip will minimize the perceived post-depositional uplift, and is therefore taken as a conservative estimate of tectonic tilt.

[48] The approximately 11 and 5 Ma paleosurfaces at the eastern limit of the Pampa del Tamarugal Basin reveal a

Table 1a. Pampa del Tamarugal Depositional and Structural Inclinations of Basin Fill: Modern Depositional Angles for Stream Channels in the Study Area

	Distance Reported (km)	Surface Angle (deg)
Chipana	3	1.8
Guatacondo	3	1.8
Maní	3	2
Sipuca	3	1.6
de Sama	3	2
Tambillo	3	1.8
Mean		1.8
±1 SD		0.2

progressive decrease in dip from the older stratigraphic units to the youngest, from a mean of 4.4° ± 1.2° for the top of the AdP to 2.6° ± 0.2° for the top of the Arcas unit, along four roughly parallel profiles that are perpendicular to the regional tectonic and topographic strike (Tables 1a–1c and Figure 8). Compaction rotation of the Altos de Pica Formation during burial beneath the Arcas unit would have caused a small amount of rotation (Text S1, section S1.2), whose subtraction from the current slope leads to the estimate that 4.2 ± 1.2° is the compaction-corrected average slope atop AdP deposits (Tables 1a–1c and Figure 5b). Because the Arcas unit is not buried, no burial compaction correction is needed for its top slope. Given the interpretation that their depositional angles were similar to that of the modern fans, the difference between the primary depositional dip (1.8 ± 0.2°) and the current dip of these compaction-corrected surfaces represents tectonic rotation (Tables 1a–1c). No clear north-south trend of the magnitude of tectonic rotation of either surface is detected.

[49] Post-depositional rotation of these Miocene surfaces is summarized in Figure 5b (see Tables 1a–1c for uncertainties, omitted temporarily for clarification of the concepts). Tectonic rotation of 1.6° occurred between ~11 and ~5 Ma. Onlap of the Arcas unit thus took place atop an AdP that was inclined at an average angle of 3.4°. Since ~5 Ma, an additional rotation of 0.8° affected the ~11 Ma top of AdP as well as the Arcas unit, bringing the angles to the modern values.

[50] The lower, western hinge of the west vergent monoclinal fold (Figure 5a) lies throughout the study area at an elevation between approximately 1500 and 1750 m (Figure 7). The eastern limit of the monocline occurs at an elevation of approximately 4300 m within the study area. Together, the mapped positions of the two hinges (Figure 7) reveal a minimum rotational wavelength of 29.3 km ± 1.6 km (λ of Figure 5a; see Tables 1a–1c).

[51] As both the lower limb of the monocline (Figure 5) and the depositional profile of the modern alluvial surface (Figure 9) involve a decrease in inclination from east to west, it is important to consider whether the westward decrease in inclination of the paleo-surfaces (Figure 9) was produced by the original depositional profile or by long-wavelength folding. Note that the dimensions of the changes in the depositional profile differ from those of the paleosurface. Measured with respect to the point where a modern channel transitions from confined to unconfined morphol-

Table 1b. Modern Slopes of Ancient Depositional Surfaces, Based on Four Profiles That Combine Surface and Seismic Data[a]

	Deviation From Strike (deg)		~5 Ma Surface		AdP Thickness (m)			~11 Ma Apparent Dip at Surface b (deg)	~11 Ma Surface Outcrop True Dip	Compaction Rotation Delta[b] (deg)	~11 Ma Surface Corrected for Compaction b′ (deg)
	Seismic Section	Outcrop Section	Apparent Dip a (deg)	True Dip	A	at 11 Ma A′					
Seismic line											
99-06	82	80	2.5	2.4	1270	1320		5.6	5.52	0.1	5.39
99-07	77	70	2.8	2.8	799	826		5.3	4.98	0.3	4.67
99-09	90	89	2.4	2.4	874	915		2.9	2.86	0.2	2.70
99-10	87	87	2.8	2.8	744	770		4.0	4.02	0.1	3.90
Mean			2.6	2.6				4.4	4.35	0.2	4.17
±1 SD			0.2	0.2				1.3	1.17	0.1	1.15
Assigned uncertainty										0.2	1.18

[a]The "a" and "b" are inclinations of the surfaces abandoned at ~5 and ~11 Ma, respectively; "A" and "A" are the current and decompacted thicknesses, respectively, of the entire Altos de Pica Formation at the location of the western monoclinal fold axis. Compaction was calculated based on the work by *Sclater and Christie* [1980] and *Allen and Allen* [1990] using N. Cardozo's freeware OSXBackstrip, with initial porosity of 35% and a "c" value of 0.4 (see Text S1 and Figure S1); "delta" represents the change in angle of the top surface of the AdP caused by compaction of the AdP unit during deposition of Arcas unit; "b" illustrates the angle of the top of the AdP derived by subtracting the compaction rotation value from the observed modern surface slope; "lambda" is the wavelength over which uplift estimates were applied.

[b]Absent data for either the primary or final porosity or C values, a systematic compaction uncertainty exists which we assign as equal to the mean value of delta, 0.2°. We choose this large value of uncertainty because at one extreme, there might have been no compaction rotation, and at the other extreme the surface porosity might have been greater or the compaction trajectory more pronounced than we tested.

Table 1c. Structural Relief Development Resultant From Postdepositional Rotation, Corrected for Compaction for Four Seismic Lines[a]

	Width of Monocline Lambda (km)	Current Inclination Post-~5 Ma	Compaction Corrected Post-~11 Ma	Depositional Dip Corrected		Structural Relief Added Across Monocline		
				Post-~5 Ma	Post-~11 Ma	Post-~5 Ma	Post-~11 Ma	Between 11 and 5 Ma
Seismic line								
99-06	30	2.44	5.39	0.64	3.59	335	1882	1547
99-07	30	2.76	4.67	0.96	2.87	503	1505	1002
99-09	30.5	2.35	2.70	0.55	0.9	293	479	186
99-10	27.5	2.81	3.90	1.01	2.1	485	1008	524
Mean	29.3	2.59	4.17	0.79	2.37	404	1219	815
±1 SD variance	1.6	0.23						
Fractional uncertainty						0.39	0.51	0.8
Uncertainty			1.18	0.30	1.20	157	621	641

[a]Uncertainties on deposition-corrected inclinations are the square root of the sum of the squares for standard deviations on current dips and depositional dips. Uncertainties on post-5 and post-11 Ma structural relief are from the square root of the sum of the (squared tangent of the fractional uncertainty on the corrected dips and squared fractional uncertainty on the monocline width). Uncertainty on the uplift between 11 and 5 Ma is from the square root of the sum of the squares of the uncertainties on the post-5 and post-11 Ma reliefs.

ogy, which is the eastern limit of a depositional profile (Figure 9), the depositional slope diminishes westward gradually by an average of 1.2° (range 1.1–1.4°) within a distance of ~4–8 km. In contrast, the paleo-surface overlying the Altos de Pica Formation diminishes its inclination about 20 km (range 14–23 km) west of its eastern limit, and does so by an average of 2.2° (range 1.3–4.2°) (relying on the depth conversions of seismic data, shown in the subsurface of Figure 8). We reason that the major hinge expressed in the seismic data is too far from the apex of the corresponding paleo-fans to attribute it to the original fan profile. Further, we hypothesize that the original position of the break-in-slope corresponding to the westward decline in depositional slope of the AdP is embedded within the monocline limb (Figure 8); note that for sections a, b, and c, the top of AdP is more steeply inclined within the easternmost 3 km of its outcrop limit than it is farther west. Regarding the top of the Arcas unit, its inclination declines at an average distance of 8 km (range 3.1–12.9 km) west of its eastern limit, by 0.6° (range 0.5–0.7°). These values overlap more substantially with those of the modern depositional profiles.

[52] These geometric relationships yield a total tectonic uplift of 1220 ± 620 m since ~11 Ma (Tables 1a–1c), partitioned between 810 ± 640 m of topographic uplift between ~11 and 5 Ma, and 400 ± 160 m of topographic uplift between ~5 Ma and the present (see Tables 1a–1c for clarification of the estimated uncertainties). These translate to a mean rate of uplift of the eastern margin of the AdP outcrop belt of 130 ± 110 m/Myr between ~11 and 5 Ma, and of 80 ± 30 m/Myr since ~5 Ma (Table 3). Given the uncertainties on geometry that are stated as well as uncertainties on the age of the top of the AdP (Text S1, section S1.1), these rates are indistinguishable. The uncertainties reported here take into consideration the variability of measured values of paleo-surface inclinations, of depositional slopes, and of the monocline width, as well as the variability of estimates of compaction (Tables 1a–1c and Text S1, section S1.2). Although the uncertainty on the magnitude of structural relief development between 11 and 5 Ma is large, the general nature of the change in landform between ~11 and 5 Ma is uniform throughout the Western Andean Slope in the study area.

6.5. Uncertainty

[53] Figure 8 reveals that the apparent depth to the ~11 Ma horizon, determined from the seismic profiles, increases systematically to the west, continuing the trend visible in outcrop. This suggests that any error in the stacking velocities is consistent among nearby shot points. The magnitude of the systematic error is best discerned in the zone of overlap between seismic profiles collected on uplands and the outcrop in nearby parallel deep canyons. For two profiles with one or two kilometers of overlap between the subsurface and surface data (Figures 8c and 8d), we see that the estimated position in depth of the easternmost location of the mapped ~11 Ma reflector is 80 m (±70 m) deeper than the projected position based on westward extension along a line of constant dip from the surface outcrops. This implies strongly that, for those locations, the true velocity is less than the stacking velocity, resulting in an overestimate of the reflector depth by ~35–140%. Because this uncertainty would propagate to an even larger uncertainty on the tectonic rotation and calculated relief growth, we *do not use* the subsurface apparent dip of the top of the AdP in the rotation analysis. Instead, we use only the present dip of the top of the AdP where it is exposed in outcrop, which constitutes the majority of the profile width for which we have constraints (Figure 8). We use the subsurface inclinations only to find the locations of the lower hinge of the monocline.

[54] The amount of compaction that influenced the Altos de Pica Formation during burial beneath the Arcas unit is poorly constrained, because the depositional porosity, final porosity, and diagenetic history are all unknown. Nevertheless, because little compaction would have been induced by the small mass of the Arcas unit, the compaction uncertainty of 0.2° contributes little to the overall uncertainty on the relief growth.

7. Description and Analysis of the Salar de Atacama basin (~22°50′S–23°50′S)

7.1. Landform

[55] The Salar de Atacama is perched on a topographic platform located at a much greater distance from the trench

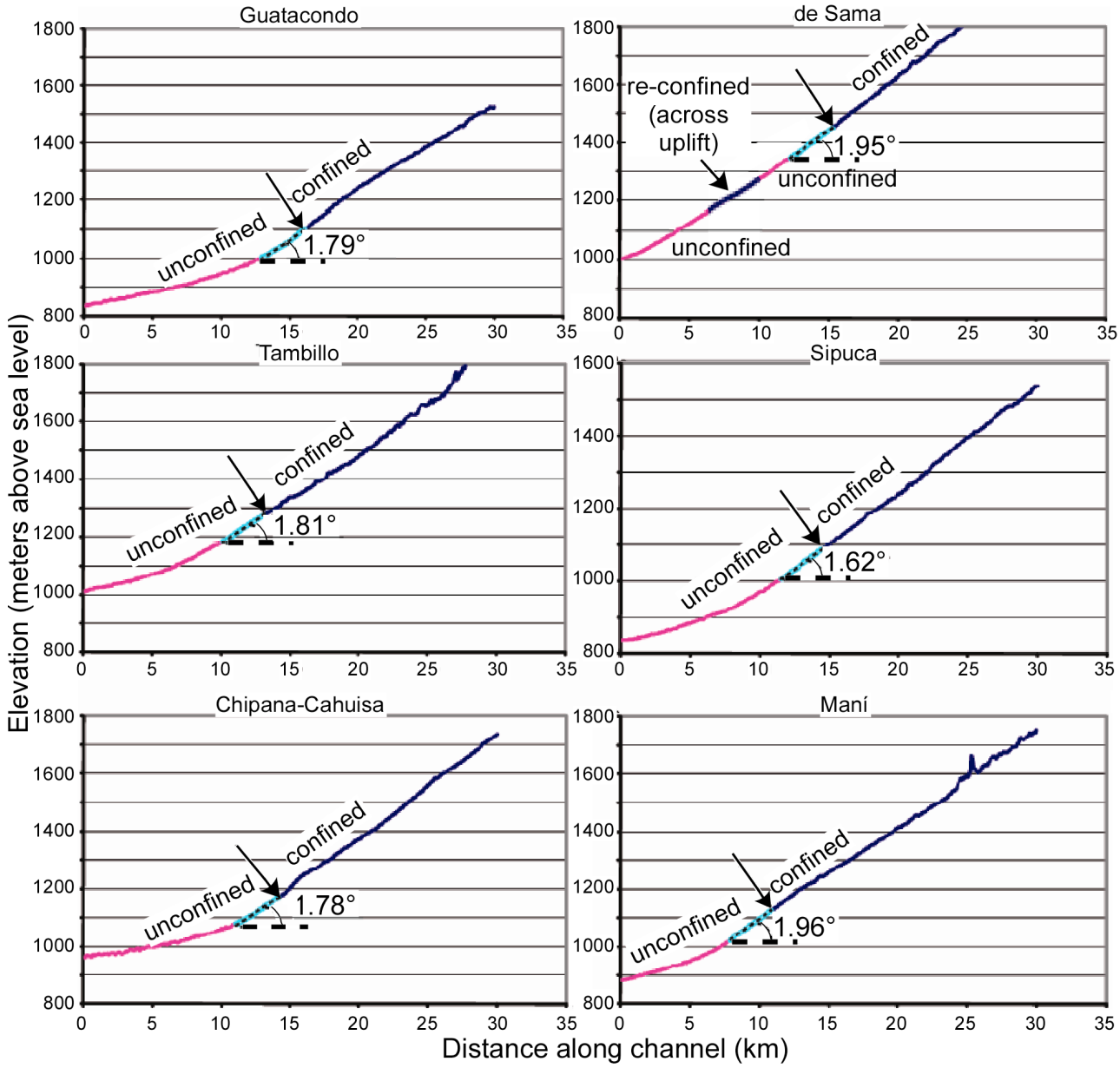

Figure 9. Longitudinal channel profiles for the six catchments used to determine the depositional angle for the modern alluvial system (locations shown on Figure 7). The arrow indicates the point at which the channel becomes unconfined downstream. For the depositional angle, a linear best fit line (dashed black line) was generated for the first 3 km (light blue line) of the unconfined segment of the channel. The angle this line makes with the horizontal is noted for each channel.

(300 km) than is the Pampa del Tamarugal (~180 km) and is 1300 m higher in elevation (Figures 2 and 3). The Western Andean Slope east of the Salar de Atacama is a simple west dipping plane, whose upper limit ranges from just over 5000 m elevation in the north to about 4400 m in the south. The lower limit of the east branch of the Western Andean Slope is the Atacama salar (salt pan), at 2300 m elevation (Figure 3). An alluvial apron between the salt plan and ~2500 m elevation provides the superficial transition between the horizontal basin and the Western Andean Slope. At elevations midway between the toe and crest (i.e., in the range of 3000–4000 m above sea level), the long-wavelength slopes (pixel size 21 × 21 km) are ~4° [*Hoke*, 2006]. Most of the Western Andean Slope is covered by Pliocene and Quaternary ignimbrites (Figure 6d) [*Ramírez and Gardeweg*, 1982] that are part of the Altiplano-Puna Volcanic Complex [*de Silva*, 1989]. Large stratovolcanoes and small lava domes sit in isolation on top of this westward-inclined surface at a variety of elevations [*Ramírez and Gardeweg*, 1982]. *Hoke* [2006] showed that the monocline here has the least dissected form of any location along the west flank of the Andes.

[56] The Western Andean Slope adjacent to the northern half of the salar is a remarkably simple tilted plane, hence we focus north of 23°30′S. In contrast, adjacent to the southern half of the salar, the Western Andean Slope is a more complicated feature. To a first order it is also a west dipping plane spanning from 2500 m to about 4400 m above sea level, but the stratovolcanoes are both so large and so abundant that they dominate the surface morphology, and numerous north trending fault scarps with vertical displacements of tens to hundreds of meters form a set of steps in elevation [*Ramírez and Gardeweg*, 1982]. The strike of the long-wavelength westward-tilted surface varies from north to south, as part of a broad arc of the Andean front around the Salar de Atacama basin. North of 23°10′S the strike is ~N15°W, between this latitude and 23°35′S the strike is ~N0°W, and south of 23°35′S the long-wavelength landscape strikes N20°E. Large uncertainty exists about the geomorphic history of the landforms east of the Salar de Atacama for times earlier than about 5 Ma, because the large volume Pliocene and Quaternary ignimbrites obscure virtually all older rocks [*Ramírez and Gardeweg*, 1982; *de Silva*, 1989].

7.2. Stratigraphy

[57] *Muñoz et al.* [2002], *Jordan et al.* [2002, 2007], *Pananont et al.* [2004], *Mpodozis et al.* [2005], *Reutter et al.* [2006], and *Arriagada et al.* [2006] have recently summarized the stratigraphic and structural evolution of the Salar de Atacama, for which they integrated extensive subsurface data with outcrop data. For consistent usage of stratigraphic terminology and because the units of interest to this study are only those of the Neogene, we draw principally upon the work of *Jordan et al.* [2002, 2007]. Two thick Miocene to Holocene units, identified as seismic stratigraphic sequences "L" (older) and "M" (younger), reach a sum of about 2500 m thickness in the mid-line of the Salar de Atacama (Figures 6d and 10).

[58] Unit "L" is the upper part of a unit ("K") that in total encompasses Oligocene to middle Miocene strata [*Jordan et al.*, 2007]. Unit K is very difficult to subdivide in the northwestern part of the basin where there are outcrops with age constraints but also complex faults and folds and poor quality seismic data. In contrast, below the salar L is separated from the lower part of "K" by an unconformity, and spans approximately ~17–10 Ma [*Jordan et al.*, 2007] (see the auxiliary material for a discussion of the uncertainty on this age). The geometry of unit L is simple: it is lenticular, thinning gradually to the east and more abruptly to the west (Figures 6d and 10). Unit L corresponds to the depth range between 980 m and approximately 1800 m in the Toconao-1 borehole where the dominant lithology is claystone, with minor sandstone and anhydrite. The western limit of L has been uplifted along the margin of the Cordillera de la Sal (Figures 6d and 10), which is the locus of salt deformation and underlain at depth by a tectonic thrust system [*Pananont et al.*, 2004; *Reutter et al.*, 2006].

[59] Unit M, dominated by halite, constitutes approximately the uppermost kilometer of strata throughout the area of the Salar de Atacama (Figure 10). Unit M contains interbeds of ignimbrites, which are the dominant feature of the surface geology of the Western Andean Slope immediately east of the salar where they are well dated. The tentative recognition of some ignimbrites in upper unit L as well as within unit M indicates that the top of L is younger than the oldest major late Cenozoic ignimbrite, which leads to the interpretation that the base of M is between 5 and 10 Ma [*Jordan et al.*, 2002].

[60] This succession of sedimentary horizons preserves the Miocene and Pliocene landforms that existed within the Salar de Atacama sedimentary basin, and we track the long-wavelength deformation of two paleo-surfaces, one whose age is ~17 Ma (base of unit L) and one ~10 Ma (base of unit M). The environment in which the halite of unit M accumulated is interpreted to have been an evaporite salt pan [*Lowenstein et al.*, 2003], while the environment for underlying unit L was a clastic playa or mudflat [*Muñoz et al.*, 2002; *Jordan et al.*, 2007]. These are environments in which the primary depositional dip would have been approximately horizontal. Broader information about the facies distribution throughout the Salar de Atacama basin and to its west indicates that the drainage basin has been closed since the Oligocene [*Reutter et al.*, 2006; *Jordan et al.*, 2007]. We can treat non-horizontality of horizons within units L and M as evidence of post-depositional tilting.

7.3. Short-Wavelength Deformation, Basin-Scale Subsidence, and Non-Tectonic Rotation

[61] Five types of relief development may have played a role in the modern geometry of Miocene to Quaternary strata in the Salar de Atacama basin. First, Salar de Atacama displays a significant degree of Miocene-Quaternary deformation across high-angle reverse faults [*Jordan et al.*, 2002, 2007]. Second, the western flank of the basin displays spectacular examples of deformation due to gravitational instability of thick Oligocene salt deposits [*Pananont et al.*, 2004]. Third, there may have been tectonic subsidence at the wavelength of the full sedimentary basin that would contribute to the creation of structural relief that is measured along horizons of known age [*Reutter et al.*, 2006; *Jordan et al.*, 2007]. Fourth, given a thickness of Cenozoic deposits within this basin that exceeds 3000 m locally and varies spatially, differential burial compaction may have added a significant magnitude of westward rotation. The mass of these sedimentary rocks would also be at least partially compensated by isostatic subsidence. Fifth, there has been long-wavelength westward rotation of the eastern flank of the basin, which is the focus of this analysis, and is treated in the following section. Here we briefly review the nature and magnitude of the first four categories of deformation. More detail is provided in the Supplementary Data.

[62] Two principal zones of short-wavelength deformation have been strong controls on the net distribution of strata within the Salar de Atacama basin since the Oligocene. Near the centerline in the southern part of the basin is the blind, north trending, west-side-up Salar Fault System (Figure 10). The second zone of significant Neogene deformation is the Cordillera de la Sal along the western margin of the salt pan.

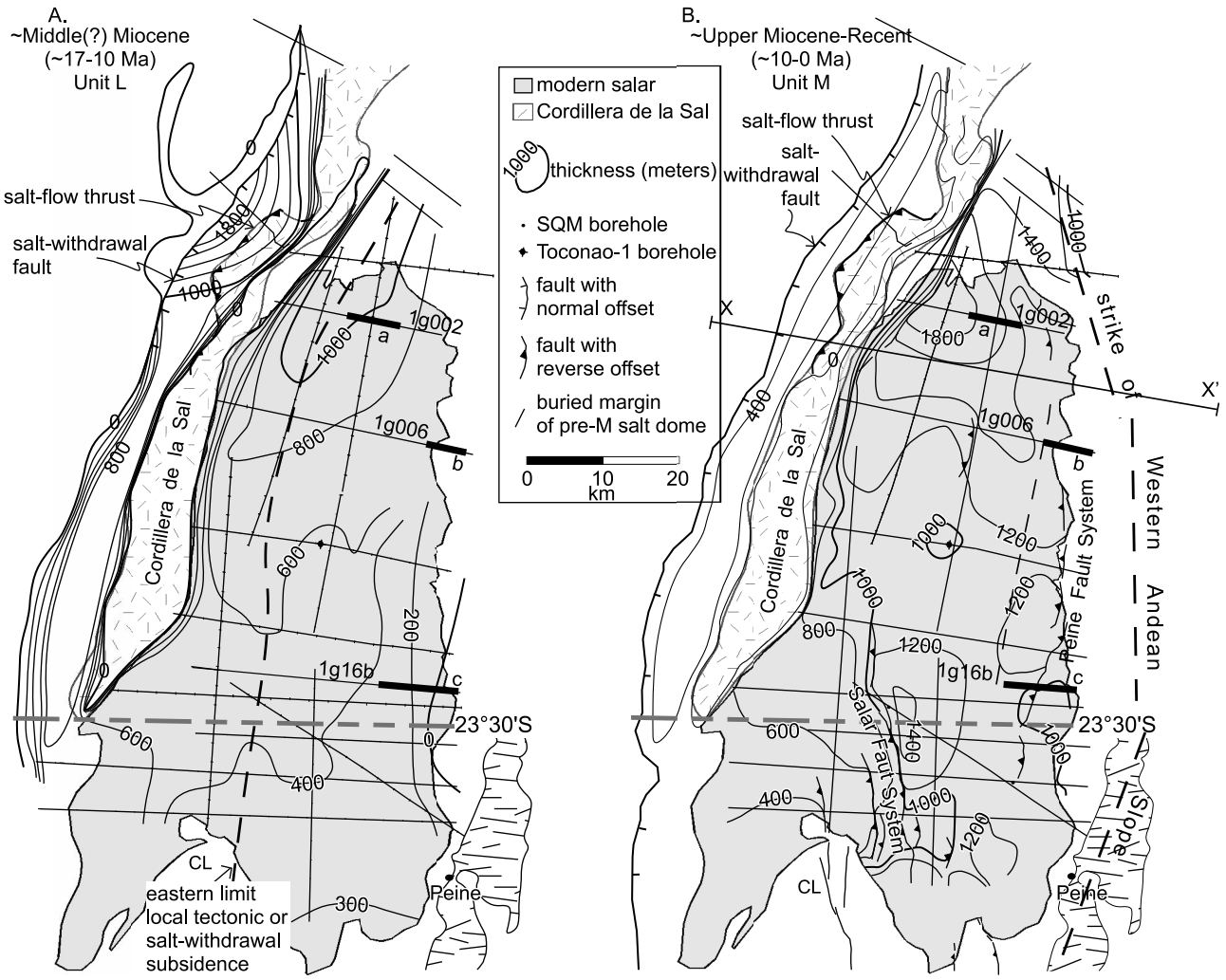

Figure 10. Isopach maps for units M [from *Jordan et al.*, 2007] and L in the Salar de Atacama basin. The locations of seismic lines on which *Jordan et al.* [2002], *Pananont et al.* [2004], and *Jordan et al.* [2007] based their analyses are shown, plus the locations of seismic lines 1g002, 1g006, and 1g16b, whose results are key to this study. Line segments "a," "b," and "c" show the sections that have west dipping inclinations that we relate here to the long-wavelength Western Andean Slope. CL marks the peninsula of the Cordón de Lila.

7.3.1. High-Angle Reverse Faults Within the Basin

[63] The thickness pattern of unit M is markedly affected by the north trending Salar Fault System that roughly bisects the southern third of the salar. Unit M's thickness changes by some 600–800 m across the Salar Fault System (Figure 10). The principal fault in the Salar Fault System has a geometry that is nearly vertical but slightly reverse, and elevates the basement of the western block by ~900 m total [*Jordan et al.*, 2002]. This important Salar Fault System is part of a family of north trending faults that were active between the late Miocene and Holocene [*Ramírez and Gardeweg*, 1982] south of 23°28′S. These include a set of faults within the Cordón de Lila peninsula which bisects the south end of the salar, the multiple reverse faults in the valley southwest of Peine, the ridge of basement rocks immediately east of Peine, a series of fault-bounded strongly tilted Miocene strata 10–20 km east of Peine, and the Miscanti fault which impounds Lake Miscanti at the western margin of the Puna plateau. Although only the offset on the blind Salar Fault System is well documented, a widespread set of landforms and faults reveals that the Western Slope is not a simple monocline here. Nearly all of these moderate- to large-offset reverse faults display east directed vergence and thus act to uplift the basin (western) end of the Western Andean Slope in opposition to the long-wavelength rotation. Back-tilting in the hanging wall of these individual blocks would increase westward tilting locally. Thus we will confine our analysis of rotation patterns and their interpretation in terms of monoclinal structural relief development to the area north of 23°28′S, where these faults do not occur.

[64] In the northern part of the basin, unit L thins abruptly to the margin of the Cordillera de la Sal. *Pananont et al.* [2004] deduced that there may have been offset along a reverse fault that underlies the Cordillera de la Sal during

this time interval. *Jordan et al.* [2007] interpreted that the Cordillera de la Sal rose to or above the depositional surface during unit L time. In summary, we conclude that the thinning west of the dashed line in Figure 10 is likely related to the Cordillera de la Sal local tectonic and salt-flow phenomena.

[65] Along the full north-south extent of the eastern border of the salar, a set of small offset reverse faults (Peine fault system) raise the western block, and thus are antithetic to the main topographic gradient from the Altiplano-Puna plateau to the salar. These faults, which typically affect thickness patterns by tens of meters, were active largely while unit L accumulated, and also disrupt the lower part of unit M.

[66] In the southern half of the basin, unit L's thickness pattern (Figure 10a) reveals no localized depocenters and therefore little or no tilting by differential tectonic subsidence *within* the Salar de Atacama basin. The pattern also reveals a small magnitude of thinning to the east that is at least in part due to onlap across a pre-existing topography [*Jordan et al.*, 2007]. However, for the northern half of the basin the thickness pattern of L (Figure 10) reveals subsidence of the midline of the salar (dashed heavy line, Figure 10) relative to the eastern border of the salar, consistent with the long-wavelength tilt of the basin due to either regional long-wavelength rotation of the Western Andean Slope and/or differential compaction of underlying strata.

[67] Even at distances of over 10 km from the two major local-scale faults (i.e., Salar Fault System and Cordillera de la Sal), unit M measures greater than 1000 m thick throughout the eastern half of the salar (Figure 10). Similarly, geometries of M imaged in the seismic data show no sign of short-wavelength footwall tilting at distances greater than ~7–10 km east of either the eastern border of the Cordillera de la Sal or of the northern tip of the Salar Fault System.

[68] Consequently, we interpret that the unit M thickness pattern beneath the eastern salar is not diagnostic of any local fault control on subsidence. Unit M persists at ~1000-m thickness of salar facies until it reaches the location of interfingering with ignimbrite sheets that continue eastward to the crest of the Altiplano-Puna plateau (Figure 6d). We postulate that the tilt of the eastern part of the basin during the accumulation of unit M reflects regional long-wavelength rotation of the Western Andean Slope and/or differential compaction of underlying strata of the Salar de Atacama basin.

7.3.2. Salt Tectonics

[69] Salt tectonics are responsible for thousands of meters of structural relief along the northwestern margin of the Salar de Atacama basin [*Pananont et al.*, 2004]. During both L and M times, salt-withdrawal subsidence and salt-tectonic uplift occurred near the Cordillera de la Sal. However, review of the ~700 km of high-resolution seismic reflection profiles distributed across the salar (Figure 10) found no evidence of salt tectonic deformation elsewhere [*Jordan et al.*, 2007].

[70] Well-documented salt diapirism during unit L time within the Cordillera de la Sal was supplied by salt withdrawal from the underlying Oligocene-lower Miocene unit K (Paciencia Group), which caused significant subsidence of the basin within a few kilometers east and west of the diapirs [*Dingman*, 1962; *Wilkes and Görler*, 1988; *Pananont et al.*, 2004]. The progressive onlap and deformation of unit L against the eastern flank of Cordillera de la Sal [*Jordan et al.*, 2007, Figure 8e] would account for much of the abrupt unit L thinning at the western margin of the salar (Figure 10a). Likewise, adjacent to the northwestern M depocenter (Figure 10b) a large degree of migration of salt occurred during unit M time, but the relative contributions to that depocenter of salt flow compared to tectonics are uncertain [*Pananont et al.*, 2004; *Reutter et al.*, 2006] (Figure 10b). Only where the trend of the Cordillera de la Sal converges with the trend of the Western Andean Slope in the northernmost Salar de Atacama basin is there overlap that interferes with our analysis of rotation related to the Western Andean Slope. Consequently, the Cordillera de la Sal salt-withdrawal effect as well as its tectonic fault may include profile "a" of our new data set, but profiles "b" and "c" are distant from the local effects of that faulting and salt tectonics (Figure 10).

7.3.3. Tectonic Subsidence of the Full Width of the Salar de Atacama

[71] The great thickness of Neogene and Quaternary strata in the Salar de Atacama basin indicates that there probably was net tectonic subsidence of the basin as a whole during the Cenozoic. For example, a ~2500 m thick package of nonmarine Paleogene strata now occurs ~500 to ~3000 m below sea level under the center of the basin (Figure 6d). It is nearly impossible to quantify the magnitude or time of net basin-wide tectonic subsidence of Oligocene or younger age because the major Oligocene phase of tectonic subsidence created a closed drainage basin which has persisted to the present [*Pananont et al.*, 2004; *Reutter et al.*, 2006; *Jordan et al.*, 2007]. In such an internally drained basin all of the strata are nonmarine, irrespective of whether the basin floor was above or below sea level, and thus there is no reference horizon for absolute subsidence. Indeed, part of the explanation of the great thickness (~1000 m) of dominantly evaporite basin fill during the last ~10 Ma is that the closed topographic low trapped all solutes in groundwater, leading to ascent of the depositional surface irrespective of descent of the basement. It is further difficult to quantify within-basin middle Miocene and younger tectonic subsidence because the basin was a topographic low created by Oligocene-early Miocene extension [*Pananont et al.*, 2004; *Jordan et al.*, 2007]. We cannot document what fraction of middle Miocene to Holocene thickness was caused by passive filling of a pre-existing valley.

7.3.4. Compaction Rotation and Isostatic Subsidence due to the Mass of Accumulating Strata

[72] Because thousands of meters of strata underlie units L and M [*Jordan et al.*, 2007], there is a likelihood that progressive compaction of those underlying strata occurred under the added burial load of units L and M. The amount of rotation that can be caused by this compaction is proportional to a) the difference in thickness of the strata underlying the western end of a given profile compared to the eastern end of that profile, b) the difference in thickness of units L and M at the western and eastern points (Figure 6d), as these are the added mass which drives compaction, and c)

the initial surface porosity and curve of porosity loss with depth. Units between the Cretaceous rocks and lower unit K thicken westward below the central part of Salar de Atacama (Figure 6d; units H-K) and therefore their compaction may have contributed to the westward tilt of the base of unit L and base of unit M. In Text S1 and Table S2, we explore in depth the plausible magnitude of compaction rotation.

[73] Isostatic subsidence under the considerable mass of the thick basin fill could cause subsidence in a sea level reference frame. Because the thickness of basin fill increases toward the west in each profile, local isostatic compensation of the mass could enhance the westward rotation and would add to rotation of the basement. One can readily calculate the plausible maximum contribution of local isostatic compensation by assuming Airy compensation and create an estimate for the westward rotation that would result from differential compensation of the eastern and western ends of our seismic data profiles. However, the isostatic subsidence probably is not locally compensated but instead is regionally compensated by flexure, considering *Schurr and Rietbrock*'s [2004] demonstration that Salar de Atacama is a cold and rigid lithospheric block. The implication is that the true westward isostatic rotation is of lower magnitude than that computed from local compensation. We do not attempt to further constrain a numerical estimate for isostatic tilting because the uncertainty of the physical premise, of local compensation rather than flexural (regional) compensation, introduces errors that exceed other sources of uncertainty, such as the spatial variability of unit thickness and the uncertainty on the selected densities. Instead of introducing a correction as part of the inclination analysis, we calculate the plausible maximum subsidence at the western hinge of the monocline, assuming Airy compensation, and consider the added uncertainty that this introduces in the final interpretation of the magnitude of tectonic uplift across the monocline (Tables 2 and 3). Calculation of the local isostatic subsidence is part of a conservative approach to estimation of tectonic subsidence, but we do not advocate that these are accurate values of subsidence under the mass of the sedimentary rocks in the Salar de Atacama basin.

7.4. Uncertainties on the Interpretation of Regional Tilting of the Salar de Atacama Basin

[74] Uncertainties include the interpretation of the seismic stratigraphy, seismic velocities, burial compaction parameters, isostatic subsidence parameters, the structural interpretation, and the primary depositional dip. In Text S1, section S2.3, we treat the uncertainties on the seismic velocities and compaction parameters, and their impacts on tilt, through numerical experimentation with a range of plausible values. The other categories of uncertainties are subject to qualitative assessment, described here.

[75] As illustrated by *Jordan et al.* [2002, 2007] the quality of seismic reflection data for Salar de Atacama is excellent. We had available for interpretation processed data displayed on a combination of paper copies and as Powerpoint slides, all of which lack stacking velocity data. It is possible to tie all the east-west oriented seismic lines available for this study through intersections with tie lines. The bases of units M and L have been mapped independently by N. Muñoz and TEJ and reconciled [*Muñoz et al.*, 2002; *Jordan et al.*, 2002, 2007], but we cannot rule out a one-cycle (~40–50 ms) or two-cycle miscorrelation at some point over the 47 km that separate the northernmost and southernmost lines whose data we present. Error in correlation will affect a comparison of tilts at various latitudes. In addition, the ability to accurately trace reflectors within a single seismic line affects accuracy of measurement of the magnitude of tilt of those surfaces. For Salar de Atacama, the quality of the data diminishes toward the eastern extreme where the long-wavelength rotation occurs. Uncertainties in tracing either the base of M or the base of L could be as much as ~100 ms. For M, which has a thickness of about 700–1000 ms in the parts of the seismic lines reported here, this would produce an error of 10–14%. For unit L, whose thickness varies between approximately 250 and 750 ms, this uncertainty could produce an error as large as 40%.

[76] The uncertainty on the structural interpretation is "unknowable." We are seeking structural tilts at the borders of the seismic data set, and we have no subsurface information beyond the limits of those seismic data. For profiles b and c (Figure 10), the locations of the 7–10 km wide segments with simple westward tilt are in themselves the strongest reason to consider them to be part of the monocline: they are contiguous with the landform that is the Western Andean Slope itself. For these two examples, the eastern limit of the seismically imaged inclined zone is the eastern limit of the seismic data, located low on the alluvial fans. But for profile a, the inclined strata are approximately 6 km west of the eastern limit of the seismic line and slightly farther from the toe of the alluvial fans. The inclined zone is limited to its east by a zone of horizontal reflections, which might be either caused by localized deformation along the Peine fault system, or may be related to a large structure. In the former case, we would choose to extrapolate the dips defined in the inclined zone across the whole width of the monocline; in the latter case we should disregard these data, like we do for lines in the southern sector of the salar where local structural tilting overwhelms the regional signal.

[77] An additional structural uncertainty comes from the three-dimensional form of the Western Andean Slope around the Salar de Atacama basin. Near the north end of the Salar de Atacama, where profile "a" (seismic line 1g002) images westward-inclined surfaces, the exposed slopes trend NW (Figure 3), whereas throughout the data set farther south the exposed slopes trend N. This causes added uncertainty in inclusion of data from profile "a."

[78] Because there are only shallow boreholes along the eastern margin of the salar, we cannot be certain that the facies encountered at the Toconao-1 borehole exist in profiles "a," "b," and "c." Hence we cannot know that the primary depositional dips of units L and M were horizontal. Cores to a few hundred meters depth within a few kilometers of profile "c" reveal dominant halite and gypsum, providing general support for our assumption that salar and playa depositional environments for unit M persist to depth under profiles "a," "b," and "c" [*Bevacqua*, 1991]. That there would be an extensive lacustrine zone with a hori-

Table 2. Growth of Structural Relief Resulting From Postdepositional Rotation, Corrected for Compaction, for Three Eastern Salar de Atacama Profiles[a]

	Monocline Width (in Seismic and to Miscanti Fault) (km)	Current Inclination		Compaction Corrected (c = 0.4)		Structural Relief Across Monocline			Reduced Tectonic Relief if Maximum Plausible Isostatic Subsidence Considered[b]		
		Post-~10 Ma M Dip of Surface	Post-~17 Ma L (deg)	Post-~10 Ma M Dip of Surface	Post-~17 Ma L (deg)	Post-~10 Ma M (m)	Post-~17 Ma L (m)	Between ~17 and 10 Ma	Post-~10 Ma M (m)	Post-~17 Ma L (m)	~17-10 Ma L-M (m)
Seismic line											
1g006	46	4.8	8.0	3.5	7.0	2939	5908	2969	1898	4220	
1g002	53	3.2	7.4	2.2	6.6	1831	5549	3718	767	3356	
1g16b	46	3.4	5.1	2.6	4.8	2195	4033	1838	1433	2871	
Mean	48.3	3.8	6.8	2.8	6.1	2322	5163	2842	1366	3482	2117
1 SD	4.0	0.9	1.5	0.7	1.2	565	995		568	683	
Uncertainties											
For maximum compaction uncertainty = 19% of uplift						441	981				
Considering velocity (see Table S3)						952	2055				
Considering velocity and compaction[c]						1049	2277	2507			
Considering isostatic subsidence under load of basin fill									1193	2377	2660
Fractional uncertainty						0.45	0.44	0.88	0.87	0.68	1.26

[a]Estimates of the potential maximum contribution of isostatic subsidence under the weight of the strata filling the basin are explored for the reduced tectonic relief. Assume that sonic velocities from Toconao-1 borehole are applicable throughout eastern salar.

[b]Assume local isostatic compensation of western end of the monoclinal profile. Assumed densities: unit M 2.0 g/cm^3 (halite), unit L 2.3 g/cm^3 (mudstone), asthenosphere 3.3 g/cm^3.

[c]Square root of the sum of the squares of the uncertainties on uplift due to compaction and velocity, which encompass the uncertainty on width.

Table 3. Summary of Tectonic Relief Development of the Western Flanks of the Altiplano and Puna Relative to the Fore Arc Basins

	Western Margin of the Altiplano					
	~26–11 Ma	± Uncertainty[a]	11 to 5 Ma	± Uncertainty[b]	5 to 0 Ma	± Uncertainty[b]
Pampa del Tamarugal basin						
Relief developed (m)	2000	500	810	640	400	170
Relief development rate (m/Myr)	130		135	110	80	31
	Western Margin of the Puna					
	~17 to 10 Ma	± Uncertainty[b]	~10 to 0 Ma	± Uncertainty[b]	~6 to 0 Ma	
Salar de Atacama basin: east branch of Western Andean Slope						
Relief developed (m)[c]	2840	2510	2320	1050		
Relief development rate (m/Myr)	410	360	230	100		
Atacama block (west branch of Western Andean Slope)						
Relief developed (m)					≤900	?
Relief development rate (m/Myr)					≤150	
Sum of west and east branches of Western Andean Slope						
Relief developed (m)	2840	2510	≤3220	?		
Relief development rate (m/Myr)	410	360	<320	?		

[a]Uncertainty on early middle Miocene short-wavelength monoclinal uplift reports the variation in ranges resolved by *Farías et al.* [2005] , *Victor et al.* [2004], and this study (the latter based on the difference between the actual topographic relief and the structural relief accounted for by post-11 Ma rotation.
[b]Uncertainty reported incorporates uncertainties on seismic velocities and compaction but does not quantify uncertainties on the geologic interpretation of the seismic data. Rate uncertainties derived by multiplying the rate by the fractional uncertainties on the uplift magnitudes (Tables 1a–1c and 2).
[c]From the "structural relief across monocline" in Table 2.

zontal primary dip, and that the lacustrine zone onlapped the toe of the monocline progressively as time passed, is a logical outcome in a closed drainage basin as the depositional surface rose. If, instead, units L or M of profiles "a," "b," and "c" accumulated as alluvial fan deposits, by analogy to slopes of the alluvial fans now fringing the salar, their primary dips would have been as much as 2°. Propagated through the calculations, for the Toconao-1 velocities, compaction estimated for c = 0.4, and including all three profiles (e.g., Table 2), if the primary dip were 2° then the best estimate of the relief increase during deposition of M would be only 630 m (compared to ~2320 m if initial condition was horizontal), and since initiation of unit L would total 3460 m (compared to 5160 m if initial condition was horizontal). We do not propagate this uncertainty below because we consider the available subsurface data to strongly support a near-horizontal primary depositional slope in the area of our seismic data.

7.5. Results: Tilted Long-Wavelength Surfaces and Surface Uplift

[79] Both the major boundaries of units M and L (Figure 6d) and many reflectors within them increase in separation to the west in a fan-like geometry [see also *Reutter et al.*, 2006], which indicates that long-wavelength tilting was contemporaneous with accumulation of those two units, rather than pre-depositional or post-depositional. In the northern half of the Salar, where there is little effect of the short-wavelength basement reverse faults, the east ends of three seismic lines reveal that the bases of units M and L are inclined several degrees to the west over distances of 7–10 km (Figures 6d and 10 and Table 2). To a first approximation, the base of unit M is co-linear with the topographic profile of the Western Andean Slope. Like for the Pampa del Tamarugal, we use the history of development of the sub-M and sub-L surfaces as a measure of the evolution of the topography of the Western Andean Slope.

[80] Depth calculations made assuming the sonic velocities documented in the Toconao-1 borehole [*Jordan et al.*, 2007, Figure 4] (Table S3) indicate that below the eastern salar the base of unit M displays 3.8° ± 0.9° of long-wavelength tilt to the west, and the base of L tilts 6.8° ± 1.5°. Based on a scenario that maximizes compaction rotation (see the auxiliary material), compaction is estimated to have introduced westward tilt whose mean is 1.1° ± 0.3° for unit M and 0.7° ± 0.4° for unit L (Table S2). Discounting from the gross rotation by this compaction rotation as well as the possible depth conversion errors introduced by the need to apply sonic velocities from a single borehole (Table S3), the rotation results in an estimated long-wavelength structural relief increase of 2320 ± 1050 m and 5160 m ± 2280 m for the bases of units M and L, respectively (Table 2).

[81] The assignment of part of that structural relief to tectonics and part to differential isostatic subsidence driven by the mass of the basin has been crudely examined (Table 2). The assumption of local compensation produces upper limits for isostatic adjustment of 960 m (during M accumulation) and 1680 m (since the beginning of L accumulation). If this isostatic compensation contributes to the structural offset, then the remaining part, at least 1370 m ± 1190 m of relief formation synchronous with unit M and ~3480 ± 2380 m of relief increase since initiation of unit L, appear to be of long-wavelength tectonic origin. At this point, the uncertainties have grown to be large fractions of the best estimates of the uplift values without even encompassing the core uncertainty

about the appropriateness of the assumed local isostatic compensation. We do not consider the isostatic effects further.

[82] Because the uncertainties are many and possibly large, we consider the timing and amount of monoclinal relief formation west of the northern Puna based on the numerical values developed in this study to be only an approximation of the first-order signal and general age range of structural relief development. In general the seismic data show a progressive rotation of the strata near the eastern margin of the Salar de Atacama basin, creating a westward fanning of horizons in units L and M, and the available chronology [*Jordan et al.*, 2002, 2007] indicates that these units span the middle Miocene through Quaternary. The magnitude of growth of relief during the middle Miocene, as well as during the late Miocene and Pliocene, was of kilometer scale, and rates were hundreds of meters per million years (Table 3).

8. Description and Analysis of the Calama Basin (22°S–23°S)

[83] A longer-wavelength (125–200 km) west dipping ancient landscape is visible between 22°S and 24°S (Figures 3 and 4). *Hoke* [2006] noted that the distribution of long-wavelength slopes could be viewed as if the Andean mountain front splits into two parts. The western, subdued and discontinuous branch of the Western Andean Slope is the western flank of the Cordillera Domeyko, a set of deeply eroded discontinuous mountains (Figure 2), remnant from mountain building during the Eocene and Oligocene [*Maksaev and Zentilli*, 1999]. This long-wavelength slope drapes *Schurr and Rietbrock*'s [2004] NW-trending strong and cold Atacama lithospheric block near 22°30′S (Figure 2), and is immediately adjacent to this 70-km-wide lithospheric block at 23°30′S. The ~50 km wavelength eastern branch of the Western Andean Slope rises to the northern Puna plateau immediately east of the Atacama block.

[84] We hypothesize that the surface uplift of the Calama and Salar de Atacama basins to intermediate altitudes (Figures 3 and 4) is contemporaneous with long-wavelength rotation of the western branch of the Western Andean Slope, and that this rotation may be genetically connected to the Atacama lithospheric block. We deduce from Calama basin Miocene strata that extend over an east-west distance of ~90 km a few basic constraints on the very long wavelength tilt across the west branch (Figures 3c and 6c). After brief treatment of the eastern branch, we focus on the western branch.

[85] The Calama basin has been defined by *May et al.* [1999] to extend from ~68°20′W to 69°15′W, based on the distribution of the tens-of-meters thick Pliocene strata that cap most of the basin. *Jordan et al.* [2006] considered the Calama basin to be only the region between ~68°20′W and 68°55′W at whose center there is a depocenter with over 2000 m thickness of Cenozoic strata. For our current purpose, we adopt *May et al.*'s [1999] broader usage.

[86] Subsurface and surface stratigraphic data for the east side of the Calama basin demonstrate a relationship to the eastern branch of the Western Andean Slope similar to that of the Pampa del Tamarugal and Salar de Atacama basins. However, only a single appropriately oriented, good-quality seismic reflection profile permits definition of the eastern margin strata, and resolves only the position at depth of a single dated unit whose depositional inclination we can estimate. This stratigraphic reference is the ~20 Ma El Yeso Formation, comprised of ~30–60 m of sandstone and well-bedded gypsum. The depositional environment was a salar, or salt pan [*Blanco*, 2008], to which we assign an initial depositional surface tilt of 0°. The overlying strata that are involved in this rotation are alluvial fan deposits, whose depositional angle we cannot estimate with confidence (Text S1, section S3.1). For this single cross section, the width of the eastern branch of the Western Andean Slope is uncertain both because extensive Pliocene to Quaternary volcanic edifices cover its eastern side and because of local deformation (Figure 6c); we estimate the plausible range as 23 km to more than 35 km. The El Yeso Formation dips 3° toward the west across the lower 11 km of the slope. Using simple geometric relationships and considering the uncertainty on the monocline width, this implies that the structural relief produced may have been 1520 m ± 440 m, or more, since ~20 Ma.

[87] The only additional age resolution of the time of relief development comes from *Blanco*'s [2008] observation that a greater proportion of detrital sediments entered the basin from the eastern flank between 10 and 6.5 Ma than had been true during the middle Miocene. *Blanco* [2008] interprets the late Miocene increase in clastic material as indicating significant contemporaneous relief development along the eastern flank of the Calama basin as a result of displacement on the east vergent fault system east of the Calama basin depositional systems (Figure 6c, dashed fault; see Text S1, section S3.2). How much of the post-20 Ma westward tilting identified in the El Yeso unit is a result of this reverse fault system, which is largely covered by volcanic rocks, and how much is a result of long-wavelength monoclinal folding along the east branch of the Western Andean Slope, is uncertain.

[88] Uncertainties on this eastern Calama basin result are significant. We lack sufficient along-strike information about the geometry of the basin fill to use statistics of variability to assess the uncertainty on the magnitude of tilt. This is especially limiting because the long-wavelength topography of the Calama basin is complex and very three-dimensional (Figure 3a). In specific, the eastern slope of the Calama basin strikes NE to NNE, even though the eastern branch of the Western Andean Slope at this latitude strikes NNW, which also suggests that displacement along faults east of the basin contributes to the documented structural relief.

[89] The western part of the Calama basin drapes the western, subdued and discontinuous branch of the Western Andean Slope. Because the western branch of the Western Andean Slope is on strike with the single-strand Western Andean Slope farther north (Figure 3), at least some part of the relief development history of the western arm of the Calama basin may have been shared with the long-wavelength monoclinal structure to its north. *Mortimer* [1980] first suggested that the westward tilt of the western

arm of the Calama basin may reflect a long-wavelength rotation that uplifts the Atacama-Calama block to its intermediate elevation (Figure 4), and *Houston et al.* [2008] proposed that the tilting occurred during the late Miocene to Pliocene.

[90] In the latest Miocene and Pliocene, 6–3 Ma, deposition was more widespread in the Calama basin (Opache Formation) than at any prior time, spanning ~100 km throughout the lowlands of the Calama Valley and stretching both northward and westward in long fingers that follow the course of the Loa River. This depositional system included a low energy axial transport system (trending south and west) amidst floodplains with a high groundwater table that led to extensive wetlands and shallow lakes [*May et al.*, 1999; *Houston et al.*, 2008; *Rech et al.*, 2010]. *May et al.* [1999] and *Blanco* [2008] interpret that the latest Miocene-Pliocene basin was internally drained, with its western boundary west of the preserved Opache pinch out (Figure 6c, arrow). Apparently, a high concentration of carbon in the groundwater facilitated widespread deposition of carbonate as paleosols, wetland deposits, lake deposits, and carbonate cement of the siliciclastic detritus [*May et al.*, 1999; *Blanco*, 2008; *Rech et al.*, 2010]. After 3 Ma, the Calama basin drainage became connected to the Pacific Ocean and base level was lowered across the Calama basin [*May et al.*, 1999; *Blanco* 2008; *Houston et al.*, 2008].

[91] Relief development is suggested in the modern distribution of the 6–3 Ma Opache Formation. A surface constructed on the preserved top of the Opache is now a simple plane inclined 1.3°W along the western branch of the basin, whereas it is approximately horizontal in the main Calama basin (Figure 6c). Because the Opache limestones accumulated in wetlands as well as shallow, ephemeral lakes, we cannot be sure which parts of its surface were horizontal at the time of its accumulation. Almost certainly some of it was not horizontal, as the lacustrine and palustrine limestones grade to carbonate-cemented sandstone and conglomerate near the bounding highlands. Indeed, even though the basin was sedimentologically internally drained, it was apparently hydrographically open, likely via groundwater flow, to the Pampa del Tamarugal to the west where a contemporaneous fluvial-lacustrine system developed at the southwestern extreme of that basin [*Sáez et al.*, 1999]. This implies that some topographic relief must have existed between the Calama basin and the Pampa del Tamarugal by 5.8 Ma, the age by which fluvial-lacustrine facies in the southern Pampa del Tamarugal basin indicate water seepage from the Calama basin area [*Sáez et al.*, 1999].

[92] As a maximum estimate for the structural relief development of the Opache Formation since the beginning of accumulation of the Opache ~6 Ma, we calculate the vertical relief that could be attained by 1.3° westward rotation, if the Opache Formation had been horizontal originally. Over a ~40 km width, from the horizontal toe-of-slope west of the western terminus of the Opache, to the eastern horizontal Calama region, this rotation would produce ~900 m of relief. *Houston et al.* [2008] used similar reasoning to conclude that there had been less than 1° of westward rotation since 3.3 Ma. Together, their study and ours agree that there could not have been more than ~900 m of new relief generated across the Cordillera de Domeyko block in which the Calama basin is embedded relative to the Central Depression during the last 6 Ma.

[93] *Rech et al.* [2006] documented Miocene and Quaternary paleosols located along the SE flank of the Calama basin, a region that now sits on the same topographic platform as the central Calama basin and western Salar de Atacama basin (Figure 4). Based on the succession of paleoclimate states indicated by superimposed types of soils, they inferred that there must have been at least 900 m of topographic uplift relative to sea level between 9.4 Ma and the Quaternary. While neither our method using the Opache Formation nor *Rech et al.*'s [2006] approach is a precise description of very long-wavelength uplift of the western branch of the Western Andean Slope, together they imply that a significant amount of the relief formation and uplift of the Atacama block is younger than 10 Ma and that at least part of this rise in elevation is due to tilt.

9. Discussion

[94] This study complements prior ones that reveal that relief development occurred during the Neogene across the western flank of the Andes over an along-strike distance of ~1000 km (~16°–24°S) [*Wörner et al.*, 2002; *Farías et al.*, 2005; *Schlunegger et al.*, 2006; *Hoke et al.*, 2007; *Thouret et al.*, 2007; *Schildgen et al.*, 2007, 2009b]. Our new data, combined with the documentation of early and middle Miocene structural relief growth by *Farías et al.* [2005], *Pinto et al.* [2004], *García and Hérail* [2005] and *Victor et al.* [2004], resolve that large magnitude tectonically produced structural relief growth along the western flank of the Altiplano and Puna plateau was underway during the early and middle Miocene, during the late Miocene, and during the Pliocene-Quaternary.

[95] *Evenstar et al.* [2009] pointed out the uncertainty of use of the relict pediplain of the Western Andean Slope as a single reference horizon for analysis of the duration of relief development, because the pediplain exhibits a multiphase history. *Riihimaki et al.* [2006] also demonstrated a multiphase history of a somewhat similar low relief surface in the Rocky Mountains. We agree with *Evenstar et al.*'s [2009] recognition of multiple landscape stages in the pediplains and depositional surfaces of the eastern Pampa del Tamarugal (Figure 7), as did *Hoke et al.* [2004, 2007]. *Hoke et al.* [2007] used the configuration of stream profiles, an independent approach, to assess the magnitude of landscape rotation, and found that there had been ~1100 m of surface uplift of the eastern side of the Pampa del Tamarugal relative to the basin over some period of time. *Hoke et al.* [2007] used a generalization of the age of the pediplain, that it was younger than the age of the strata which underlie it, to provide a time constraint on the stream profile disturbance, and thus estimated the age of landscape rotation to be less than ~10 Ma. Our newly reported results (Tables 1a–1c) for the southern Pampa del Tamarugal basin refine the chronology of *Hoke et al.* [2007] but arrive at a strikingly similar magnitude (~1200 m since ~11 Ma) through an independent methodology. We conclude that this study of kinematic markers and stratigraphic data demonstrates that an aggregate

stream profile history for the last ~10 Ma [*Hoke et al.*, 2007] provides a valid history of relief development. The results obtained from different methods converge because the magnitude of surface changes across the eastern sectors of the Pampa del Tamarugal landscape related to the climate variability of the last 10 Myr has been small (e.g., tens of meters vertical change) outside of the incised canyons, roughly two orders of magnitude less than the relief development across the western slope. The long-term hyperarid climate has diminished the importance of a suite of competing processes and enabled acquisition of a robust history of surface relief development over millions of years time span.

[96] Our objective is to compare the histories of surface uplift west of the Altiplano and west of the Puna, but in order to arrive at those histories from our relief growth measures we must reference our data to an absolute frame; that is, we must estimate the contribution of absolute tectonic subsidence in the fore-arc basins studied. The internal geometry of the Pampa del Tamarugal fore-arc basin indicates that it underwent little or no tectonic subsidence since the end of deposition of the Altos de Pica Formation [*Nester*, 2008], in which case the relief formation measurements equate to tectonic uplift. Furthermore, given the absence of significant denudation of the pediplains outside of the canyons [*Kober et al.*, 2007; *Evenstar et al.*, 2009], the tectonic uplift equates to surface uplift. In the fore-arc area west of the western branch of the Western Andean Slope, 22°S–24°S, sediment accumulation is negligible, a fore-arc basin does not occur, and climate is hyperarid. Relief formation along the western branch, then, likewise can be equated to tectonic rock and surface uplift.

[97] In contrast, in the Salar de Atacama basin the isopach patterns of unit M and large magnitude faults that control its distribution are unambiguous evidence that tectonic subsidence of this fore-arc basin was a factor during the late Miocene–Quaternary [*Reutter et al.*, 2006; *Jordan et al.*, 2007]. Consequently, we lack a confident reference frame against which to transform the late Miocene–Quaternary relief growth of the eastern branch of the Western Andean Slope to surface uplift. We note that the relief generation west of the Puna (~2320 ± 1050 m) is estimated to be twice as much as the tectonic relief generation (in that case, surface uplift) west of the Altiplano (~1220 ± 620 m) since 10–11 Ma (Tables 1a–1c and 3) and that the Puna plateau surface currently is indeed at a higher elevation than the Altiplano.

9.1. Spatial Variability of Surface Relief Development History

[98] Late Miocene uplift of the Western Andean Slope (Figure 11b) was vigorous adjacent to the southern Altiplano (800 ± 600 m), and its accommodation by a long-wavelength monocline mimicked the style of structural relief generation begun earlier at the margin of the northern Puna. Adjacent to the northern Puna, the eastern branch of the Western Andean Slope was similarly or possibly more active, accruing as surface uplift some fraction of the 2300 ± 1000 m of structural relief that formed post-10 Ma. The similarity of style adjacent to the Puna and Altiplano is noteworthy, and might not have been predicted given the rheological differences that are expected from the differing magmatic histories of the southwestern Altiplano plateau compared to the northern Puna plateau [*Trumbull et al.*, 2006]. The northwestern Puna and transition to the Altiplano plateau, adjacent to the Calama and Salar de Atacama basins, were inundated in the great ignimbrites of the Altiplano Puna Volcanic Complex (APVC, Figures 1 and 2) [*de Silva*, 1989] from 10 to 1 Ma, but this surface expression of extensive crustal melting did not persist far northward where the Altiplano is adjacent the Pampa del Tamarugal basin; *de Silva et al.* [2006] note that geophysical data suggest that a mid-crustal magma body [*Zandt et al.*, 2003] underlies not only the APVC but also extends at least another 100 km northward in the western part of the Altiplano, which might indicate a rheological similarity. However, the seismological and gravity data measure a modern zone of mid-crustal partial melt which may or may not have existed during the late Miocene.

[99] Despite the co-linearity of the Western Slope adjacent the Altiplano and of the western branch of the Western Slope adjacent the northern Puna (Figures 2 and 3), their uplift histories and mechanisms differ. For example, for the middle Miocene the western flank of the Domeyko Range lacks relief-forming short-wavelength monoclinal folds and faults [*Marinovic et al.*, 1995; *Marinovic and García*, 1999; *Marinovic*, 2007] like those adjacent the Altiplano. The western branch is also co-linear with the single-thread Western Andean Slope south of ~25°S [*Isacks*, 1988; *Hoke*, 2006] (Figure 3). At the latitude of Copiapo (26–28°S), geomorphic evidence suggests ~800–1000 m of post 10-Ma relief development along the Western Andean Slope adjacent the southern Puna [*Mortimer*, 1973; *Riquelme et al.*, 2007], comparable to the magnitude adjacent the southern Altiplano.

[100] An explanation for the bifurcation into two Western Slope branches west of the northern Puna may be related to the Atacama lithospheric block, which neighbors and is partially overlapped by the western branch (Figure 2) [*Schurr and Rietbrock*, 2004; *Reutter et al.*, 2006]. The Atacama block differs from the fore arc to its north and south in that its lithosphere is anomalously thick as well as cold and strong, while its intermediate composition crust is of low temperature and high pressure [*Schurr and Rietbrock*, 2004]. In gross characteristics, the Atacama block is somewhat like the Colorado Plateau of the western United States, which is a region of anomalously thick and cold lithosphere and long-lived stability. *Roy et al.* [2009] demonstrate that flexural adjustments to heat introduced at the sides of the Colorado plateau during the mid-Cenozoic ignimbrite flare-up, followed by migration over tens of millions of years of the thermal consequences toward the interior of that block, can explain the 1000–2000 m of documented late Cenozoic surface uplift. It is worth considering whether, in an analogous fashion, differential heating of the Atacama block during the Pliocene to Quaternary creation of the Altiplano Puna volcanic complex and magma body along only the eastern side [*de Silva et al.*, 2006] may have caused Pliocene-Quaternary uplift [e.g., *Rech et al.*, 2006] of the eastern side and tilt

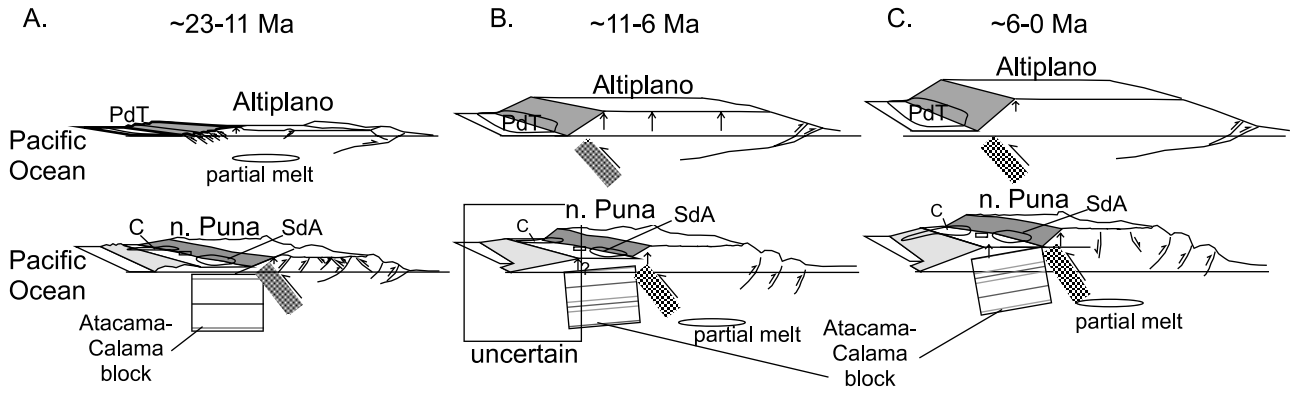

Figure 11. Cartoon comparison of historical progression of topographic uplift of the central Andes at the latitudes of the (top) Altiplano and (bottom) northern Puna plateau, during the Neogene. The diagrams emphasize the style and timing of crustal structure that accompanied uplift but are not comprehensive crustal sections and only allude to rheologic and volumetric changes controlled by magmatic activity or delamination. The timing and magnitude of uplift are based on data from this paper for the fore-arc region, and based on the work by *Garzione et al.* [2008] and *Hoke and Garzione* [2008] for the Altiplano. Timing and style of crustal structures of the fore arc are from references in text and for Altiplano, Puna, Eastern Cordillera, and Subandean domains are from *Elger et al.* [2005], *Coutand et al.* [2001], and *Rosario et al.* [2008].

toward the west. Because the available geophysical data reveal that the Atacama block is cool, it is counter-intuitive to propose its recent uplift by thermal expansion. Yet transient heat flow may have warmed the lithosphere to a temperature higher than existed during the Miocene even though still colder than the neighboring regions. *Roy et al.* [2009] demonstrate that the horizontal scale of gradient in the magnitude of uplift at the Colorado plateau margins is ~200 km, and that 500–900 m of uplift of the block edge is a reasonable consequence of 5 to 10 Myr of propagation of the marginal thermal anomaly.

[101] The fore arc adjacent both the southern Altiplano and the Puna also may have risen en masse with the plateau, as *Schlunegger et al.* [2006] suggested may have been important during the Pliocene and Quaternary. *Schildgen et al.* [2009b] document en masse uplift of the southwestern Peru fore arc by ~1 km between ~5 and 2.2 Ma (Figure 1). Unfortunately, the methods employed in this study are not sensitive to wholesale uplift of the fore arc and Altiplano-Puna plateau as a single block, unless the block tilted.

9.2. Comparison of the Relief History of the Western Andean Slope to the Altiplano Uplift History

[102] The current study complements previous studies that reveal that, between 15°S and 20°S, uplift has occurred since ~10 Ma across a ~500 km width of the central Andes (Figure 1), spanning the Western Andean Slope (uplift magnitude 1200 ± 600 m [this study]) [*Farías et al.*, 2005; *Hoke et al.*, 2007; *Thouret et al.*, 2007; *Schildgen et al.*, 2007, 2009a, 2009b], within the Altiplano plateau (magnitude ~2500 ± 1000 m [*Garzione et al.*, 2006, 2008; *Ghosh et al.*, 2006; *Gregory-Wodzicki*, 2002] or as little as 1100 ± 1600 m [*Ehlers and Poulsen*, 2009]), and including the Eastern Cordillera (magnitude 1700 ± 700 m) [*Barke and Lamb*, 2006]. In the Altiplano, proxy data are interpreted by *Garzione et al.* [2006, 2008] and *Ghosh et al.* [2006] to imply that a major phase of surface uplift *began* ~10 Ma, the same time as (1) cessation of short-wavelength deformation along the Western Andean Slope [*Farías et al.*, 2005; *Victor et al.*, 2004], (2) the end of significant deformation within the Altiplano [*Elger et al.*, 2005], and (3) a shift in foreland deformation from the Eastern Cordillera to the Subandean fold-and-thrust belt [*Gubbels et al.*, 1993; *Echavarría et al.*, 2003]. Viewed from the Altiplano and Eastern Cordillera, *Gubbels et al.* [1993] and *Garzione et al.* [2006, 2008] suggest that a fundamental change in mountain building style occurred at ~10 Ma. Viewed from the Western Andean Slope, likewise a change of deformation style is evident at ~10 Ma. Following the cessation of short-wavelength deformation in northern Chile, west of the Altiplano, long-wavelength monoclinal tilting began and affected a narrow belt traceable at least from southern Peru (~18°S) to 27°S and likely beyond [*Isacks*, 1988; *Hoke* 2006]. This late Miocene long-wavelength monoclinal deformation extended far beyond the limits of the early middle Miocene short-wavelength deformation, affecting areas where little or no early or middle Miocene vertical displacement is recorded, such as the western branch of the Western Andean Slope adjacent the northern Puna [this study] and the Western Andean Slope adjacent the southern Puna [*Mortimer*, 1973; *Riquelme et al.*, 2007]. Yet at the latitude of the southern Altiplano and northern Puna, there was no significant change near 10 Ma in the rate of development of structural relief (Table 3).

[103] We designed this analysis to provide a conservative estimate of tectonic relief development, and adopted assumptions that would minimize the tectonic relief. For example, we use a primary depositional inclination for alluvial strata that is appropriate to proximal alluvial fans, and we assume large degrees of differential compaction. Thus the results (Table 3) are best estimates of minimum tectonic relief development.

[104] It remains ambiguous whether the magnitude of post-10 Ma uplift of the Altiplano exceeds that of the Western Andean Slope. In part the ambiguity results from different measurement methods, paleoaltimetry for the Altiplano compared to structural relief growth measurements for the fore-arc studies. Based on this study's and *Hoke et al.*'s [2007] results, it appears that there was either ~1300 m less [*Garzione et al.*, 2006, 2008; *Ghosh et al.*, 2006] or an equal amount [*Ehlers and Poulsen*, 2009] of uplift of the western border of the Altiplano compared to the Altiplano proper since ~10 Ma. Perhaps more important than the uncertainties on our best estimates, our studies of fore-arc relief development do not encompass altitudinal increase that might explain the ~1000 m of relief between sea level and the west side of the Pampa del Tamarugal fore-arc basin (western scarp of Figure 4), which is expressed in the spectacular Coastal Escarpment. If uplift younger than 10 Ma were responsible for this relief, as *Schildgen et al.* [2009b] demonstrate some 500 km farther north, then the altitudinal increase of the western lip of the Altiplano is of roughly similar magnitude as the larger estimates for the central sector of the Altiplano. The age of the Coastal Escarpment is problematic, and many prior workers consider the relief to be relict from the Paleogene [e.g., *Mortimer and Sarič*, 1975]. Although *Schlunegger et al.* [2006] bracketed between ~8 and 3 Ma the uplift of one northern Chile river system relative to the Pacific Ocean where there is no Coastal Escarpment, the applicability of their result regionally is not clear to us.

9.3. Tectonic Causes for Surface Uplift

[105] Much has been written about the tectonic mechanisms for surface uplift of the Altiplano and Eastern Cordillera [e.g., *Isacks*, 1988; *Gubbels et al.*, 1993; *Allmendinger et al.*, 1997; *Victor et al.*, 2004; *Elger et al.*, 2005; *Barke and Lamb*, 2006; *Garzione et al.*, 2006, 2008; *Molnar and Garzione*, 2007; *Hoke and Garzione*, 2008; *Kay and Coira*, 2009; *DeCelles et al.*, 2009; *Barnes and Ehlers*, 2009]. As direct controls on uplift, three processes compete as candidates for the uplift since ~10 Ma. *Barke and Lamb* [2006] point to the underthrusting of the Brazilian shield as the key driver for uplift. *Garzione et al.* [2006, 2008], *Molnar and Garzione* [2007], and *Hoke and Garzione* [2008] counter that the pace of Altiplano uplift exceeds what could be driven by underthrusting of the shield. Instead, they consider delamination of the eclogitic lower crust beneath the plateau [*Kay and Kay*, 1993; *Kay et al.*, 1994; *Schurr et al.*, 2006] to have been the principal mechanism for rapid uplift of both the Altiplano and the Puna. Flow of lower crustal rock from the Western Cordillera and Eastern Cordillera into the Altiplano may have caused uplift of the Altiplano [*Husson and Sempere*, 2003], though at the expense of crustal thickness and elevation of the Western Cordillera.

[106] From the perspective of the Western Andean Slope, a mechanistic tie of the late Miocene-Pliocene uplift to underthrusting of the Brazilian shield is problematic. The magnitude of underthrusting of the Brazilian shield along the eastern Andean thrust belts diminishes south of the Altiplano [reviewed in *Allmendinger et al*., 1997; *Kley and Monaldi*, 1998], which is evidenced in the loss of a thin-skinned thrust belt adjacent to the Puna plateau (Figure 1). While our data include substantial uncertainty on the magnitude of surface uplift of the western margin of the Puna which cannot be rigorously disentangled from subsidence of the fore-arc basin, the simplest interpretation (Table 3) is that uplift of the west side of the Puna plateau has been as much as or more than uplift of the west side of the Altiplano during the Neogene. This is opposite the trend that we expect if uplift were caused primarily by underthrusting.

[107] Published analyses of delamination and underthrusting to build the Altiplano-Puna plateau [*Kay et al.*, 1994; *Garzione et al.*, 2006, 2008; *Molnar and Garzione*, 2007; *Hoke and Garzione*, 2008] integrate the role and history of vigorous arc and back-arc magmatism as important controls on rheological and density evolution. Yet at the western margin of the plateau system the magmatic addition of mass and heat to the crust may play more direct roles in surface uplift [*Victor et al.*, 2004]. There appears to be a correspondence between the along-strike change in the magnitude and style of fore-arc relief growth and the position of the APVC (Figures 1 and 2), controlled either by primary effects like buoyancy increase where the crust is heated and/or by secondary effects on rheology [*de Silva et al.*, 2006]. Work remains before the magmatic controls, lithospheric thinning controls (delamination), and crustal shortening controls are fully disentangled and documented.

[108] Large-scale geomorphology [*Isacks*, 1988], small-scale landforms (i.e., channel profiles [*Hoke et al.*, 2007]), and large-scale growth relations in Miocene to Quaternary strata in the fore-arc basins all demonstrate that surface uplift of the Andean plateau system was accommodated at its western flank by large-scale monoclinal folding. However, the uplift of major continental plateaus across long-wavelength monoclines is not treated in the literature as a widespread phenomenon. Rather than being a unique attribute of the Andes Mountains, we propose that this kinematic style of large-scale deformation likely has been common in other orogenic belts. The lack of evidence elsewhere can be attributed to the rareness of adequate preservation of the shallow upper crustal units in which it would be expressed. In northern Chile, a mere 500 m of widespread denudation would obliterate the geomorphologic record and severely limit a reconstruction of the stratal geometries, and ~1000 m of denudation would eliminate the stratigraphic record of long-wavelength growth geometries in both the Tamarugal and Calama basins. Were geologists of the future to attempt to reconstruct deformation of the western flank of a deeply denuded Andes and find only the growth-strata of the Salar de Atacama basin, they might well interpret them as a localized situation. It is only because we have the advantage of data preserved in an extraordinarily arid setting that the magnitude of a monoclinal kinematic style and its history can be fully appreciated.

10. Conclusions

[109] We conclude that there was no single, or short-lived, step in the Neogene central Andean evolution that dominated the history of relief development for the western part

of the orogenic belt [see also *Barnes and Ehlers*, 2009]. During the early and middle Miocene (Figure 11a), relief development at the western margin of the Altiplano totaled roughly 2000 m (±500 m) [*Victor et al.*, 2004; *Farías et al.*, 2005], accommodated by a set of parallel, west verging, short-wavelength monoclinal folds over small upper crustal faults. *Victor et al.* [2004] suggested that the multiple faults joined in the mid-crust with a ductile magma body. In comparison, no similar set of early and middle Miocene short-wavelength monoclinal folds is identified in the fore arc adjacent to the northern Puna. However, middle Miocene tilting of the eastern branch of the Western Andean Slope across a long-wavelength monocline seems to have created 2800 m (±400 m) of structural relief, partitioned between subsidence of the Salar de Atacama basin and surface uplift of the Andean front. During the late Miocene (~11–5.5 Ma), surface relief between the fore arc and western Altiplano plateau increased by 810 m (±640 m) (Table 3). Likewise, adjacent both the southern Altiplano and the northern Puna, topographic relief formed during the last 5 or 6 Ma (Figure 11c). Whereas the proxies used by *Garzione et al.* [2008] in the central and northern Altiplano suggest that uplift had ceased by ~6 Ma, the stratigraphic and geomorphic evidence show that the western rim of the Altiplano continued a net increase in elevation of 400 m (±170 m) during the Pliocene-Quaternary. Though we are not able to subdivide the temporal steps of the eastern branch of the Western Andean Slope structural relief growth more finely than pre- and post-10 Ma, the progressive rotation of seismic reflectors in the sedimentary package overlying the ~10 Ma marker horizon reveals that relief grew during the Pliocene-Quaternary as well as during the late Miocene.

[110] Even though the timing of relief formation of the western flanks of the southern Altiplano plateau and of the northern Puna plateau are broadly similar and both are of kilometer-magnitude (Table 3), the fore-arc basins responded in different manners (Figure 11). Fore-arc styles of deformation that contribute to relief growth include a series of west vergent near surface faults that produce small-scale monoclines where they emerge in sedimentary basins, large-scale surface rotation on one or more monoclines that include the upper crust, and wholesale uplift of the fore arc and plateau as a single unit. These deformation styles are all anticipated to have existed in other ancient fore arcs as well, prior to erasure of the evidence during denudation.

[111] **Acknowledgments.** Financial support for P.L.N., G.D.H., F.D., and T.E.J. was provided, in part, by National Science Foundation awards EAR-0208130 and EAR-0609621 to T.E.J. and for G.D.H. by NASA's NAGS-11424. Field work by N.B. and A.J.T. was supported by the Servicio Nacional de Geología y Minería, Chile. This study would not have been possible without loans of seismic reflection data by ENAP (Empresa Nacional del Petróleo, Chile) and Fred Digert (International Exploration Associates, Ltd). David Mohrig provided vital assistance in conversion of paper seismic profiles to digital format. We thank Antonio Díaz, Mario Martínez, and Hector Toro of SERNAGEOMIN for logistical support. We appreciate very much the numerous constructive suggestions of Associate Editor Todd Ehlers, Kelin Whipple, and an anonymous reviewer.

References

Allen, P. A., and J. R. Allen (1990), *Basin Analysis: Principles and Applications*, 451 pp., Blackwell Sci., Oxford, U. K.

Allmendinger, R. W., B. L. Isacks, T. E. Jordan, and S. M. Kay (1997), The evolution of the Altiplano-Puna plateau of the central Andes, *Annu. Rev. Earth Sci.*, *25*, 139–174, doi:10.1146/annurev.earth.25.1.139.

Allmendinger, R. W., G. González, J. Yu, G. D. Hoke, and B. L. Isacks (2005), Trench-parallel shortening in the northern Chilean forearc: Tectonic and climatic implications, *Geol. Soc. Am. Bull.*, *117*, 89–104, doi:10.1130/B25505.1.

Arriagada, C., P. R. Cobbold, and P. Roperch (2006), Salar de Atacama basin: A record of compressional tectonics in the central Andes since the mid-Cretaceous, *Tectonics*, *25*, TC1008, doi:10.1029/2004TC001770.

Barke, R., and S. Lamb (2006), Late Cenozoic uplift of the Eastern Cordillera, Bolivian Andes, *Earth Planet. Sci. Lett.*, *249*, 350–367, doi:10.1016/j.epsl.2006.07.012.

Barnes, J. B., and T. A. Ehlers (2009), End member models for Andean Plateau uplift, *Earth Sci. Rev.*, *97*, 105–132, doi:10.1016/j.earscirev.2009.08.003.

Beck, S., and G. Zandt (2002), The nature of orogenic crust in the central Andes, *J. Geophys. Res.*, *107* (B10), 2230, doi:10.1029/2000JB000124.

Bevacqua, P. (1991), Geomorfologia del Salar de Atacama y estratigrafia de su nucleo y delta, segunda region de Antofagasta, Chile, Masters thesis, 284 pp., Univ. Catholica del Norte, Antofagasta, Chile.

Blair, T. C., and J. G. McPherson (1994), Alluvial fans and their natural distinction from rivers based on morphology, hydraulic processes, sedimentary processes, and facies assemblages, *J. Sediment. Res.*, *64*, 450–489.

Blanco, P. N. (2008), Estratigrafía y evolución Tectono-Sedimentaria de la Cuenca Cenozoica de Calama (Chile, 22°S), M.S. thesis, 68 pp., Univ. de Barcelona, Barcelona, Spain.

Blanco, N., and A. Tomlinson (2006), Fm. Sichal: Sedimentación aluvial (Eoceno-Oligoceno) sintectónica al evento orogénico Incaico, Región de Antofagasta, Chile, *Actas Congr. Geol. Chileno*, *11*, 29–32.

Blanco, N., and A. Tomlinson (2009), Carta Chiu Chiu, Región de Antofagasta, Carta Geológica de Chile, *Ser. Geol. Básica 117*, Serv. Nac. de Geol. y Minería, Santiago.

Busby, C. J., and R. V. Ingersoll (Eds.) (1995), *Tectonics of Sedimentary Basins*, 579 pp., Blackwell Sci., Cambridge, Mass.

Carrizo, D. A., G. L. González, and T. J. Dunai (2008), Constricción Neógena en la Cordillera de la Costa norte de Chile: Neotectónica y datación de superficies con ^{21}Ne cosmogénico, *Rev. Geol. Chile*, *35*, 1–38, doi:10.4067/S0716-02082008000100001.

Castel, T., and P. Oettli (2008), Sensitivity of the C-band SRTM DEM vertical accuracy to terrain characteristics and spatial resolution, in *Headway in Spatial Data Handling*, edited by A. Ruas and C. Gold, pp. 277–296, Springer, Berlin.

Charrier, R., N. Muñoz, and S. Palma-Held (1994), Edad y contenido paleoflorístico de la Formación Chucal y condiciones paleoclimáticas para el Oligoceno tardío—Mioceno Inferior en el Altiplano de Arica, Chile, *Actas Congr. Geol. Chileno*, *7*, 434–437.

Charrier, R., L. Pinto, and M. P. Rodríguez (2007), Tectonostratigraphic evolution of the Andean orogen in Chile, in *The Geology of Chile*, edited by T. Moreno and W. Gibbons, pp. 21–114, Geol. Soc., London.

Coutand, I., P. Gautier, P. R. Cobbold, M. de Urreiztieta, A. Chauvin, D. Gapais, E. A. Rossello, and O. Lopez-Gammundi (2001), Style and history of Andean deformation, Puna Plateau, northwestern Argentina, *Tectonics*, *20*, 210–234, doi:10.1029/2000TC900031.

Davis, G. H., and S. J. Reynolds (1994), *Structural Geology of Rocks and Regions*, 2nd ed., 776 pp., John Wiley, New York.

DeCelles, P. G., M. B. Gray, K. D. Ridgway, R. B. Cole, P. Srivastava, N. Pequera, and D. A. Pivnik (1991), Kinematic history of a foreland uplift from Paleocene synorogenic conglomerate, Beartooth Range, Wyoming and Montana, *Geol. Soc. Am. Bull.*, *103*, 1458–1475, doi:10.1130/0016-7606(1991)103<1458:KHOAFU>2.3.CO;2.

DeCelles, P. G., M. N. Ducea, P. Kapp, and G. Zandt (2009), Cyclicity in Cordilleran orogenic systems, *Nat. Geosci.*, *2*, 251–257, doi:10.1038/ngeo469.

de Silva, S. L. (1989), Altiplano-Puna volcanic complex of the central Andes, *Geology*, *17*, 1102–1106, doi:10.1130/0091-7613(1989)017<1102:APVCOT>2.3.CO;2.

de Silva, S., G. Zandt, R. Trumbull, J. G. Viramonte, G. Salas, and N. Jimenez (2006), Large ignimbrite eruptions and volcano-tectonic depressions in the Central Andes: A thermomechanical perspective, in *Mechanisms of Activity and Unrest at Large Calderas*, edited by C. Troise et al., *Geol. Soc. Spec. Publ.*, *269*, 47–63, doi:10.1144/GSL.SP.2006.269.01.04.

Dickinson, W. R. (1995), Forearc basins, in *Tectonics of Sedimentary Basins*, edited by C. J. Busby and R. V. Ingersoll, pp. 221–261, Blackwell Sci., Cambridge, Mass.

Dingman, R. J. (1962), Tertiary salt domes near San Pedro de Atacama, *U.S. Geol. Surv. Prof. Pap.*, *450D*, 92–94.

Dingman, R. J., and C. Galli-Olivier (1965), Geology and ground-water resources of the Pica area, Tarapaca Province, Chile, *U.S. Geol. Surv. Bull.*, *1189*, 113 pp.

Dunai, T. J., G. A. González López, and J. Juez-Larré (2005), Oligocene–Miocene age of aridity in the Atacama Desert revealed by exposure dating of erosion-sensitive landforms, *Geology*, *33*, 321–324, doi:10.1130/G21184.1.

Echavarría, L., R. Hernández, R. W. Allmendinger, and J. Reynolds (2003), Subandean thrust and fold belt of northwestern Argentina: Geometry and timing of the Andean evolution, *AAPG Bull.*, *87*, 965–985, doi:10.1306/01200300196.

Ehlers, T. A., and C. J. Poulsen (2009), Influence of Andean uplift on climate and paleoaltimetry estimates, *Earth Planet. Sci. Lett.*, *281*, 238–248, doi:10.1016/j.epsl.2009.02.026.

Elger, K., O. Oncken, and J. Glodny (2005), Plateau-style accumulation of deformation: Southern Altiplano, *Tectonics*, *24*, TC4020, doi:10.1029/2004TC001675.

England, P., and P. Molnar (1990), Surface uplift, uplift of rocks, and exhumation of rocks, *Geology*, *18*, 1173, doi:10.1130/0091-7613(1990)018<1173:SUUORA>2.3.CO;2.

Evenstar, L. A., A. J. Hartley, F. M. Stuart, A. E. Mather, C. M. Rice, and G. Chong (2009), Multiphase development of the Atacama Planation Surface recorded by cosmogenic ^{3}He exposure ages: Implications for uplift and Cenozoic climate change in western South America, *Geology*, *37*, 27–30, doi:10.1130/G25437A.1.

Ewing, S. A., B. Sutter, J. Owen, K. Nishiizumi, W. Sharp, S. S. Cliff, K. Perry, W. Dietrich, C. P. McKay, and R. Amundson (2006), A threshold in soil formation at Earth's arid–hyperarid transition, *Geochim. Cosmochim. Acta*, *70*, 5293–5322, doi:10.1016/j.gca.2006.08.020.

Falorni, G., V. Teles, E. R. Vivoni, R. L. Bras, and K. S. Amaratunga (2005), Analysis and characterization of the vertical accuracy of digital elevation models from the Shuttle Radar Topography Mission, *J. Geophys. Res.*, *110*, F02005, doi:10.1029/2003JF000113.

Farías, M., R. Charrier, D. Comte, J. Martinod, and G. Hérail (2005), Late Cenozoic deformation and uplift of the western flank of the Altiplano: Evidence from the depositional, tectonic, and geomorphologic evolution and shallow seismic activity (northern Chile at 19°30′S), *Tectonics*, *24*, TC4001, doi:10.1029/2004TC001667.

García, M., and G. Hérail (2005), Fault-related folding, drainage network evolution and valley incision during the Neogene in the Andean Precordillera of northern Chile, *Geomorphology*, *65*, 279–300, doi:10.1016/j.geomorph.2004.09.007.

Garzione, C. N., P. Molnar, J. C. Libarkin, and B. J. MacFadden (2006), Rapid late Miocene rise of the Bolivian Altiplano: Evidence for removal of mantle lithosphere, *Earth Planet. Sci. Lett.*, *241*, 543–556, doi:10.1016/j.epsl.2005.11.026.

Garzione, C. N., G. D. Hoke, J. C. Libarkin, S. Withers, B. MacFadden, J. Eiler, P. Ghosh, and A. Mulch (2008), Rise of the Andes, *Science*, *320*, 1304–1307, doi:10.1126/science.1148615.

Ghosh, P., C. N. Garzione, and J. M. Eiler (2006), Rapid uplift of the Altiplano revealed through ^{13}C–^{18}O bonds in paleosol carbonates, *Science*, *311*, 511, doi:10.1126/science.1119365.

Gillis, R. J., and B. K. Horton (2006), Thermochronology, geochronology, and upper crustal structure of the Cordillera Real: Implications for Cenozoic exhumation of the central Andean plateau, *Tectonics*, *25*, TC6007, doi:10.1029/2005TC001887.

Gregory-Wodzicki, K. M. (2000), Uplift history of the central and northern Andes: A review, *Geol. Soc. Am. Bull.*, *112*, 1091–1105, doi:10.1130/0016-7606(2000)112<1091:UHOTCA>2.0.CO;2.

Gregory-Wodzicki, K. M. (2002), A late Miocene subtropical-dry flora from the northern Altiplano, Bolivia, *Palaeogeogr. Palaeoclimatol. Palaeoecol.*, *180*, 331–348, doi:10.1016/S0031-0182(01)00434-5.

Gubbels, T., B. Isacks, and E. Farrar (1993), High-level surfaces, plateau uplift, and foreland development, Bolivian central Andes, *Geology*, *21*, 695–698, doi:10.1130/0091-7613(1993)021<0695:HLSPUA>2.3.CO;2.

Hartley, A. J., and L. Evenstar (2010), Cenozoic stratigraphic development in the north Chilean forearc: Implications for basin development and uplift history of the Central Andean margin, *Tectonophysics*, doi:10.1016/j.tecto.2009.05.013, in press.

Hartley, A. J., G. S. Weissmann, G. J. Nichols, and G. L. Warwick (2010), Large distributive fluvial systems: Characteristics, distribution, and controls on development, *J. Sediment. Res.*, *80*, 167, doi:10.2110/jsr.2010.016.

Hindle, D., J. Kley, O. Oncken, and S. Sobolev (2005), Crustal balance and crustal flux from shortening estimates in the central Andes, *Earth Planet. Sci. Lett.*, *230*, 113–124, doi:10.1016/j.epsl.2004.11.004.

Hoke, G. D. (2006), The influence of climate and tectonics on the geomorphology of the western slope of the Central Andes, Chile and Peru, Ph.D. thesis, 283 pp., Cornell Univ., Ithaca, N. Y.

Hoke, G. D., and C. N. Garzione (2008), Paleosurfaces, paleoelevation, and the mechanisms for the late Miocene topographic development of the Altiplano plateau, *Earth Planet. Sci. Lett.*, *271*, 192–201, doi:10.1016/j.epsl.2008.04.008.

Hoke, G. D., B. L. Isacks, T. E. Jordan, and J. S. Yu (2004), Groundwater-sapping origin for the giant quebradas of northern Chile, *Geology*, *32*, 605–608, doi:10.1130/G20601.1.

Hoke, G. D., B. L. Isacks, T. E. Jordan, N. Blanco, A. J. Tomlinson, and J. Ramezani (2007), Geomorphic evidence for post-10 Ma uplift of the western flank of the central Andes 18°30′–22°S, *Tectonics*, *26*, TC5021, doi:10.1029/2006TC002082.

Hongn, F., C. del Papa, J. Powell, I. Petrinovic, R. Mon, and V. Deraco (2007), Middle Eocene deformation and sedimentation in the Puna-Eastern Cordillera, *Geology*, *35*, 271–274, doi:10.1130/G23189A.1.

Horton, B. (2005), Revised deformation history of the central Andes: Inferences from Cenozoic foredeep and intermontane basins of the Eastern Cordillera, Bolivia, *Tectonics*, *24*, TC3011, doi:10.1029/2003TC001619.

Horton, B. K., B. A. Hampton, and G. L. Waanders (2001), Paleogene synorogenic sedimentation in the Altiplano plateau and implications for initial mountain building in the central Andes, *Geol. Soc. Am. Bull.*, *113*, 1387, doi:10.1130/0016-7606(2001)113<1387:PSSITA>2.0.CO;2.

Houston, J. (2002), Groundwater recharge through an alluvial fan in the Atacama Desert, northern Chile: Mechanisms, magnitudes and causes, *Hydrol. Processes*, *16*, 3019–3035, doi:10.1002/hyp.1086.

Houston, J., D. Hart, and A. Houston (2008), Neogene sedimentary deformation in the Chilean forearc and implications for Andean basin development, seismicity and uplift, *J. Geol. Soc.*, *165*, 291–306, doi:10.1144/0016-76492007-022.

Husson, L., and T. Sempere (2003), Thickening the Altiplano crust by gravity-driven crustal channel flow, *Geophys. Res. Lett.*, *30*(5), 1243, doi:10.1029/2002GL016877.

Isacks, B. L. (1988), Uplift of the central Andean plateau and bending of the Bolivian orocline, *J. Geophys. Res.*, *93*, 3211–3231, doi:10.1029/JB093iB04p03211.

Jordan, T. E. (1981), Thrust loads and foreland basin evolution, Cretaceous, western United States, *Am. Assoc. Pet. Geol. Bull.*, *65*, 2506–2520.

Jordan, T. E., N. Blanco, F. M. Dávila, and A. J. Tomlinson (2006), Sismoestratigrafía de la Cuenca Calama (22°–23° LS), Chile, *Actas Congr. Geol. Chileno*, *11*, 53–56.

Jordan, T. E., N. Muñoz, M. Hein, T. Lowenstein, L. Godfrey, and J. Yu (2002), Active faulting and folding without topographic expression in an evaporite basin, Chile, *Geol. Soc. Am. Bull.*, *114*, 1406–1421, doi:10.1130/0016-7606(2002)114<1406:AFAFWT>2.0.CO;2.

Jordan, T. E., C. Mpodozis, N. Muñoz, N. Blanco, P. Pananont, and M. Gardeweg (2007), Cenozoic subsurface stratigraphy and structure of the Salar de Atacama Basin, northern Chile, *J. South Am. Earth Sci.*, *23*, 122–146, doi:10.1016/j.jsames.2006.09.024.

Kay, R. W., and S. M. Kay (1993), Delamination and delamination magmatism, *Tectonophysics*, *219*, 177–189, doi:10.1016/0040-1951(93)90295-U.

Kay, S. M., and B. L. Coira (2009), Shallowing and steepening subduction zones, continental lithospheric loss, magmatism, and crustal flow under the Central Andean Altiplano-Puna Plateau, in *Backbone of the Americas: Shallow Subduction, Plateau Uplift, and Ridge and Terrane Collision*, edited by S. M. Kay, V. A. Ramos, and W. R. Dickinson, *Mem. Geol. Soc. Am.*, *204*, 229–259, doi:10.1130/2009.1204(11).

Kay, S. M., B. Coira, and J. Viramonte (1994), Young mafic back arc volcanic rocks as indicators of continental lithospheric delamination beneath the Argentine Puna plateau, central Andes, *J. Geophys. Res.*, *99*(B12), 24,323–24,339, doi:10.1029/94JB00896.

Kiefer, E., M. J. Dörr, H. Ibbeken, and H. J. Götze (1997), Gravity-based mass balance of an alluvial fan giant: The Arcas Fan, Pampa del Tamarugal, northern Chile, *Rev. Geol. Chile*, *24*, 165–185.

Kley, J., and C. R. Monaldi (1998), Tectonic shortening and crustal thickness in the Central Andes; how good is the correlation?, *Geology*, *26*, 723–726, doi:10.1130/0091-7613(1998)026<0723:TSACTI>2.3.CO;2.

Kober, F., F. Schlunegger, G. Zeilinger, and H. Schneider (2006), Surface uplift and climate change: The geomorphic evolution of the Western Escarpment of the Andes of northern Chile between the Miocene and present, in *Tectonics, Climate and Landscape Evolution*, edited by S. D. Willett et al., *Spec. Pap. Geol. Soc. Am.*, *398*, 75–86.

Kober, F., S. Ivy-Ochs, G. Zeilinger, F. Schlunegger, P. W. Kubik, H. Baur, and R. Wieler (2007), Denudation rates and a topography-driven precipitation threshold in northern Chile: Multiple cosmogenic nuclide data and sediment yield budgets, *Geomorphology*, *83*, 97–120, doi:10.1016/j.geomorph.2006.06.029.

Lowenstein, T. K., M. C. Hein, A. L. Bobst, T. E. Jordan, T. L. Ku, and S. Luo (2003), An assessment of stratigraphic completeness in climate-sensitive closed-basin lake sediments: Salar de Atacama, Chile, *J. Sediment. Res.*, *73*, 91–104, doi:10.1306/061002730091.

Maksaev, V., and M. Zentilli (1999), Fission track thermochronology of the Domeyko Cordillera, northern Chile: Implications for Andean tectonics and porphyry copper metallogenesis, *Explor. Min. Geol.*, *8*, 65–89.

Marinovic, N. (2007), Carta Oficina Domeyko, Región de Antofagasta, Carta Geológica de Chile, *Ser. Geol. Básica 105*, Serv. Nac. de Geol. y Miner., Santiago, Chile.

Marinovic, N., and M. García (1999), Hoja Pampa Unión, Región de Antofagasta, *Mapas Geol. 9*, Serv. Nac. de Geol. y Miner., Santiago, Chile.

Marinovic, N., I. Smoje, V. Maksaev, M. Hervé, and C. Mpodozis (1995), Hoja Aguas Blancas, Región de Antofagasta, *Carta Geol. Chile 70*, 150 pp., Serv. Nac. de Geol. y Miner., Santiago, Chile.

May, G., A. J. Hartley, F. M. Stuart, and G. Chong (1999), Tectonic signatures in arid continental basins: An example from the upper Miocene-Pleistocene, Calama basin, Andean forearc, northern Chile, *Palaeogeogr. Palaeoclimatol. Palaeoecol.*, *151*, 55–77, doi:10.1016/S0031-0182(99)00016-4.

McGlashan, N., L. D. Brown, and S. M. Kay (2008), Crustal thicknesses in the Central Andes from teleseismically recorded depth phase precursors, *Geophys. J. Int.*, *175*, 1013–1022, doi:10.1111/j.1365-246X.2008.03897.x.

Molnar, P., and C. N. Garzione (2007), Bounds on the viscosity coefficient of continental lithosphere from

removal of mantle lithosphere beneath the Altiplano and Eastern Cordillera, *Tectonics*, *26*, TC2013, doi:10.1029/2006TC001964.

Mortimer, C. (1973), The Cenozoic history of the southern Atacama Desert, Chile, *J. Geol. Soc.*, *129*, 505–526, doi:10.1144/gsjgs.129.5.0505.

Mortimer, C. (1980), Drainage evolution in the Atacama Desert of northernmost Chile, *Rev. Geol. Chile*, *11*, 3–28.

Mortimer, C., and N. Sarič (1975), Cenozoic studies in northernmost Chile, *Geol. Rundsch.*, *64*, 395–420, doi:10.1007/BF01820676.

Mpodozis, C., C. Arriagada, M. Basso, P. Roperch, P. Cobbold, and M. Reich (2005), Late Mesozoic to Paleogene stratigraphy of the Salar de Atacama Basin, Antofagasta, northern Chile: Implications for the tectonic evolution of the central Andes, *Tectonophysics*, *399*, 125–154, doi:10.1016/j.tecto.2004.12.019.

Muñoz, N., and R. Charrier (1996), Uplift of the western border of the Altiplano on a west vergent thrust system, northern Chile, *J. South Am. Earth Sci.*, *9*, 171–181, doi:10.1016/0895-9811(96)00004-1.

Muñoz, N., R. Charrier, and T. Jordan (2002), Interactions between basement and cover during the evolution of the Salar de Atacama Basin, northern Chile, *Rev. Geol. Chile*, *29*, 55–80, doi:10.4067/S0716-02082002000100004.

Muñoz, V. A. (2007), Evolución morfoestructural del piedemonte Altiplánico Chileno deurante el Cenozoico Superior entre La Quebrada de Tarapacá y La Quebrada de Sagasca (19°45′–21°15′S), Geologist thesis, 118 pp., Univ. de Chile, Santiago.

Myers, S. C., S. Beck, G. Zandt, and T. Wallace (1998), Lithospheric-scale structure across the Bolivian Andes from tomographic images of velocity and attenuation for P and S waves, *J. Geophys. Res.*, *103*(B9), 21,233–21,252, doi:10.1029/98JB00956.

Naranjo, J. A., and R. Paskoff (1985), Evolucion Cenozoica del Piedemonte Andino en la Pampa del Tamarugal, norte de Chile (18°–21°S), *Actas Congr. Geol. Chileno*, *4*, 5.149–5.165.

Nester, P. (2008), Basin and paleoclimate evolution of the Pampa del Tamarugal forearc valley, Atacama Desert, northern Chile, Ph.D. thesis, 253 pp., Cornell Univ., Ithaca, N. Y.

Nester, P. L., E. Gayó, C. Latorre, T. E. Jordan, and N. Blanco (2007), Perennial stream discharge in the hyperarid Atacama Desert of northern Chile during the latest Pleistocene, *Proc. Natl. Acad. Sci. U. S. A.*, *104*, 19,724–19,729, doi:10.1073/pnas.0705373104.

Nishiizumi, K., M. W. Caffee, R. C. Finkel, G. Brimhall, and T. Mote (2005), Remnants of a fossil alluvial fan landscape of Miocene age in the Atacama Desert of northern Chile using cosmogenic nuclide exposure age dating, *Earth Planet. Sci. Lett.*, *237*, 499–507, doi:10.1016/j.epsl.2005.05.032.

Pananont, P., C. Mpodozis, N. Blanco, T. E. Jordan, and L. D. Brown (2004), Cenozoic evolution of the northwestern Salar de Atacama Basin, northern Chile, *Tectonics*, *23*, TC6007, doi:10.1029/2003TC001595.

Paola, C., and D. Mohrig (1996), Palaeohydraulics revisited: Palaeoslope estimation in coarse-grained braided rivers, *Basin Res.*, *8*, 243–254, doi:10.1046/j.1365-2117.1996.00253.x.

Patton, T. L. (2004), Numerical models of growth-sediment development above an active monocline, *Basin Res.*, *16*, 25–39, doi:10.1111/j.1365-2117.2003.00220.x.

Pinto, L., G. Hérail, and R. Charrier (2004), Sedimentación sintectónica asociada a las estructuras neógenas en la Precordillera de la zona de Moquella, Tarapacá (19°15′S, norte de Chile), *Rev. Geol. Chile*, *31*, 19–44, doi:10.4067/S0716-02082004000100002.

Quade, J., J. A. Rech, C. Latorre, J. L. Betancourt, E. Gleeson, and M. T. K. Kalin (2007), Soils at the hyperarid margin: The isotopic composition of soil carbonate from the Atacama Desert, northern Chile, *Geochim. Cosmochim. Acta*, *71*(15), 3772–3795, doi:10.1016/j.gca.2007.02.016.

Ramírez, C., and M. Gardeweg (1982), Hoja Toconao, Región de Antofagasta, 122 pp., Serv. Nac. de Geol. y Miner., Santiago, Chile.

Rech, J. A., B. S. Currie, G. Michalski, and A. M. Cowan (2006), Neogene climate change and uplift in the Atacama Desert, Chile, *Geology*, *34*, 761–764, doi:10.1130/G22444.1.

Rech, J. A., B. S. Currie, T. E. Jordan, and R. Riquelme (2009), The antiquity of the Atacama Desert and its implications for the paleoelevation of the central Andes, *Geol. Soc. Am. Abstr. Programs*, *41*, 523.

Rech, J. A., B. S. Currie, E. D. Shullenberger, S. P. Dunagan, T. E. Jordan, N. Blanco, A. J. Tomlinson, H. D. Rowe, and J. Houston (2010), Evidence for the development of the Andean rain shadow from a Neogene isotopic record in the Atacama Desert, Chile, *Earth Planet. Sci. Lett.*, *292*, 371–382, doi:10.1016/j.epsl.2010.02.004.

Reutter, K. J., et al. (2006), The Salar de Atacama Basin: A subsiding block within the western edge of the Altiplano-Puna Plateau, in *The Andes–Active Subduction Orogeny*, edited by O. Oncken et al., pp. 303–326, Springer, Berlin.

Riba, O. (1976), Syntectonic unconformities of the Alto Cardener, Spanish Pyrenees: A genetic interpretation, *Sediment. Geol.*, *15*, 213–233, doi:10.1016/0037-0738(76)90017-8.

Riihimaki, C. A., R. S. Anderson, E. B. Safran, D. P. Dethier, R. C. Finkel, and P. R. Bierman (2006), Longevity and progressive abandonment of the Rocky Flats surface, Front Range, Colorado, *Geomorphology*, *78*, 265–278, doi:10.1016/j.geomorph.2006.01.035.

Riquelme, R., G. Hérail, J. Martinod, R. Charrier, and J. Darrozes (2007), Late Cenozoic geomorphologic signal of Andean forearc deformation and tilting associated with the uplift and climate changes of the Southern Atacama Desert (26°S–28°S), *Geomorphology*, *86*, 283–306, doi:10.1016/j.geomorph.2006.09.004.

Rosario, J. J., J. Hernández, R. Hernández, and T. Jordan (2008), Evolución Tectono-sedimentaria durante el Terciario en la Provincia de Jujuy, in *Geología y Recursos Naturales de la Provincia de Jujuy*, edited by B. Coira and E. O. Zappettini, pp. 263–285, Congr. Geol. Argent., Jujuy, Argentina.

Roy, M., T. H. Jordan, and J. Pederson (2009), Colorado Plateau magmatism and uplift by warming of heterogeneous lithosphere, *Nature*, *459*, 978–982, doi:10.1038/nature08052.

Sáez, A., L. Cabrera, A. Jensen, and G. Chong (1999), Late Neogene lacustrine record and palaeogeography in the Quillagua-Llamara basin, Central Andean fore-arc (northern Chile), *Palaeogeogr. Palaeoclimatol. Palaeoecol.*, *151*, 5–37, doi:10.1016/S0031-0182(99)00013-9.

Schildgen, T. F., K. V. Hodges, K. X. Whipple, P. W. Reiners, and M. S. Pringle (2007), Uplift of the western margin of the Andean plateau revealed from canyon incision history, southern Peru, *Geology*, *35*, 523–526, doi:10.1130/G23532A.1.

Schildgen, T. F., T. A. Ehlers, D. M. Whipp Jr., M. C. van Soest, K. X. Whipple, and K. V. Hodges (2009a), Quantifying canyon incision and Andean Plateau surface uplift, southwest Peru: A thermochronometer and numerical modeling approach, *J. Geophys. Res.*, *114*, F04014, doi:10.1029/2009JF001305.

Schildgen, T. F., K. V. Hodges, K. X. Whipple, M. S. Pringle, M. van Soest, and K. Cornell (2009b), Late Cenozoic structural and tectonic development of the western margin of the central Andean Plateau in southwest Peru, *Tectonics*, *28*, TC4007, doi:10.1029/2008TC002403.

Schlunegger, F., G. Zeilinger, A. Kounov, F. Kober, and B. Hüsser (2006), Scale of relief growth in the forearc of the Andes of northern Chile (Arica latitude, 18°S), *Terra Nova*, *18*, 217–223, doi:10.1111/j.1365-3121.2006.00682.x.

Schurr, B., and A. Rietbrock (2004), Deep seismic structure of the Atacama basin, northern Chile, *Geophys. Res. Lett.*, *31*, L12601, doi:10.1029/2004GL019796.

Schurr, B., A. Rietbrock, G. Asch, R. Kind, and O. Oncken (2006), Evidence for lithospheric detachment in the central Andes from local earthquake tomography, *Tectonophysics*, *415*, 203–223, doi:10.1016/j.tecto.2005.12.007.

Sclater, J. G., and P. A. F. Christie (1980), Continental stretching: An explanation of the post mid-Cretaceous subsidence of the central North Sea basin, *J. Geophys. Res.*, *85*, 3711–3739, doi:10.1029/JB085iB07p03711.

Sick, C., et al. (2006), Seismic images of accretive and erosive subduction zones from the Chilean margin, in *The Andes–Active Subduction Orogeny*, edited by O. Oncken et al., pp. 147–170, Springer, Berlin.

Suppe, J., G. T. Chou, and S. C. Hook (1992), Rates of folding and faulting determined from growth strata, in *Thrust Tectonics*, edited by K. R. McClay, pp. 105–121, Chapman and Hall, London.

Taylor, J. R. (1997), *An Introduction to Error Analysis: The Study of Uncertainties in Physical Measurements*, 327 pp., Univ. Sci. Books, Sausalito, Calif.

Thouret, J. C., G. Wörner, Y. Gunnell, B. Singer, X. Zhang, and T. Souriot (2007), Geochronologic and stratigraphic constraints on canyon incision and Miocene uplift of the central Andes in Peru, *Earth Planet. Sci. Lett.*, *263*, 151–166, doi:10.1016/j.epsl.2007.07.023.

Tomlinson, A., and N. Blanco (1997), Structural evolution and displacement history of the West Fault system, Precordillera, Chile: Part 2, Postmineral history, *Actas Congr. Geol. Chileno*, *8*, 1878–1882.

Tomlinson, A. J., N. Blanco, V. Maksaev, J. H. Dilles, A. Grunder, and M. Ladino (2001), *Geologia de la Precordillera Andina de Quebrada Blanca–Chuquicamata, Regiones I y II (20°30′–22°30′S)*, 444 pp., Serv. Nac. de Geol. y Miner., Santiago, Chile.

Trumbull, R. B., U. Riller, O. Oncken, E. Scheuber, K. Munier, and F. Hongn (2006), The time-space distribution of Cenozoic volcanism in the South-Central Andes: A new data compilation and some tectonic implications, in *The Andes–Active Subduction Orogeny*, edited by O. Oncken et al., pp. 29–44, Springer, Berlin.

Victor, P., O. Oncken, and J. Glodny (2004), Uplift of the western Altiplano plateau: Evidence from the Precordillera between 20° and 21°S (northern Chile), *Tectonics*, *23*, TC4004, doi:10.1029/2003TC001519.

von Huene, R., and C. R. Ranero (2003), Subduction erosion and basal friction along the sediment-starved convergent margin off Antofagasta, Chile, *J. Geophys. Res.*, *108*(B2), 2079, doi:10.1029/2001JB001569.

von Huene, R., and D. W. Scholl (1991), Observations at convergent margins concerning sediment subduction, subduction erosion, and the growth of continental crust, *Rev. Geophys.*, *29*, 279–316, doi:10.1029/91RG00969.

von Huene, R., W. Weinrebe, and F. Heeren (1999), Subduction erosion along the North Chile margin, *J. Geodyn.*, *27*, 234–247.

von Rotz, R., F. Schlunegger, F. Heller, and I. Villa (2005), Assessing the age of relief growth in the Andes of northern Chile: Magneto-polarity chronologies from Neogene continental sections, *Terra Nova*, *17*, 462–471, doi:10.1111/j.1365-3121.2005.00634.x.

Whitman, D., B. L. Isacks, and S. M. Kay (1996), Lithospheric structure and along-strike segmentation of the Central Andean Plateau: Seismic Q, magmatism, flexure, topography and tectonics, *Tectonophysics*, *259*, 29–40, doi:10.1016/0040-1951(95)00130-1.

Wilkes, E., and K. Görler (1988), Sedimentary and structural evolution of the Cordillera de la Sal, II región, Chile, *Actas Congr. Geol. Chileno*, *1*(5), A173–A188.

Wörner, G., D. Uhlig, I. Kohler, and H. Seyfried (2002), Evolution of the West Andean Escarpment at 18°S (N. Chile) during the last 25 Ma: Uplift, erosion and collapse through time, *Tectonophysics*, *345*, 183–198, doi:10.1016/S0040-1951(01)00212-8.

Zandt, G., M. Leidig, J. Chmielowski, D. Baumont, and X. Yuan (2003), Seismic detection and characterization of the Altiplano-Puna magma body, central Andes, *Pure Appl. Geophys.*, *160*, 789–807, doi:10.1007/PL00012557.

N. Blanco and A. J. Tomlinson, Servicio Nacional de Geología y Minería, Casilla 10465, Santiago, Chile.

F. Dávila, Cátedra de Estratigrafia y Geología Histórica, Universidad Nacional de Córdoba, Pabellon Geologia, Avenida Velez Sarsfield, Córdoba X5016GCA, Argentina.

G. D. Hoke, Earth Sciences, Syracuse University, Heroy Hall, Syracuse, NY 13244, USA.

T. E. Jordan and P. L. Nester, Earth and Atmospheric Sciences, Cornell University, 2122 Snee Hall, Ithaca, NY 14853-1504, USA. (tej1@cornell.edu)